BIOPHYSICAL STUDIES OF ANHYDROUS PEPTIDE STRUCTURE

A Dissertation

by

JANEL RENEE MCLEAN

Submitted to the Office of Graduate Studies of
Texas A&M University
in partial fulfillment of the requirements for the degree of

DOCTOR OF PHILOSOPHY

August 2007

Major Subject: Chemistry

BIOPHYSICAL STUDIES OF ANHYDROUS PEPTIDE STRUCTURE

A Dissertation

by

JANEL RENEE MCLEAN

Submitted to the Office of Graduate Studies of
Texas A&M University
in partial fulfillment of the requirements for the degree of

DOCTOR OF PHILOSOPHY

Approved by:

Chair of Committee,	David H. Russell
Committee Members,	Lisa M. Pérez
	Arthur E. Johnson
	J. Martin Scholtz
Head of Department,	David H. Russell

August 2007

Major Subject: Chemistry

ABSTRACT

Biophysical Studies of Anhydrous Peptide Structure. (August 2007)

Janel Renee McLean, B.A., Maryville College;

M.S., Cornell University

Chair of Advisory Committee: Dr. David H. Russell

Defining the intrinsic properties of amino acids which dictate the formation of helices, the most common protein secondary structure element, is an essential part of understanding protein folding. Pauling and co-workers initially predicted helical peptide folding motifs in the absence of solvent, suggesting that *in vacuo* studies may potentially discern the role of solvation in protein structure. Ion mobility-mass spectrometry (IM-MS) combines a gas-phase ion separation based on collision cross-section (apparent surface area) with time-of-flight MS. The result is a correlation of collision cross-section with mass-to-charge, allowing detection of multiple conformations of the same ion. Most gas-phase peptide ions assume a compact, globular state that minimizes exposure to the low dielectric environment and maximizes intramolecular charge solvation. Conversely, a small number of peptides adopt a more extended (β-sheet or α-helix) conformation and exhibit a larger than predicted collision cross-section. Collision cross-sections measured using IM-MS are correlated with theoretical models generated using simulated annealing and allow for assignment of the overall ion structural motif (*e.g.* helix vs. charge-solvated globule).

Here, two series of model peptides having known solution-phase helical propensities, namely Ac-(AAKAA)$_n$Y-NH$_2$ (n = 3, 4, 5, 6 and 7) and Ac-Y(AEAAKA)$_n$F-NH$_2$ (n = 2, 3, 4, and 5), are investigated using IM-MS. Both protonated ($[M + H]^+$) and metal-coordinated ($[M + X]^+$ where X = Li, Na, K, Rb or Cs) species were analyzed to better understand the interplay of forces involved in gas-phase helical structure and stability. The data are analyzed using computational methods to examine the influence of peptide length, primary sequence, and number of basic (Lys, K) and acidic (Glu, E) residues on anhydrous ion structure.

This work is dedicated to my loving grandparents-

James Rozzell Kemp

Fern Bernice Walker Kemp

Ella Lee Rogers Beckley

and

Eddie Ray Beckley

(1926-1989)

ACKNOWLEDGEMENTS

First and foremost, I want to thank my family for all their loving support throughout my life and especially through many years of education. I especially want to thank my mother (Evelyn Kemp) and brothers (Jason and Steven Beckley) for always believing in me and supporting all my dreams, no matter what they were or where they might lead. I also want to thank the whole McLean clan for all their support and for raising such a wonderful, considerate man—John, my husband, closest friend and biggest supporter. John, I sincerely thank you for your love, support and strength. You've helped me become a better person and a better scientist. I am so grateful to have you as a partner in this wild ride called life. Last, I'd like to thank my closest friends who are like family to me—Rachel, Manja and Anne Marie—for listening, supporting me, making me laugh when I felt like crying, and being role models for strong, confident women everywhere.

I would like to extend my sincere appreciation to David Russell for the opportunity to work with him and profit from his wisdom, guidance and contagious enthusiasm for science. I am so thankful to have been a part of the Russell group from whom I have learned so much. I'd especially like to thank Stacy Sherrod, Stephanie Cologna, Brad Williams, Jody May and Wenjian Sun for their support in and out of the lab.

I am indebted to my advisory committee members for their input during my doctoral studies. Lisa Pérez was instrumental in the development of the simulated annealing

techniques described here and I want to thank her for her unbelievable patience, understanding and support while I learned about the world of supercomputers and UNIX. Thanks to Marty Scholtz for the peptides that spurred these studies and several exciting discussions. Thanks to Art Johnson for immediately putting me at ease during my first days at Texas A & M and supporting my scientific development both in and out of the MB program. Last, although not officially a member of my committee, I'd like to thank Nice Pace for his insightful perspectives and stimulating discussions.

My scientific curiosity has grown from interactions with a number of wonderful people outside Texas A & M as well. I'd like to thank my high school biology teacher, Miss Fain, for awakening and nurturing my love for nature. I sincerely thank my college chemistry professors, Terry Bunde, Bob Naylor and Kim Frederick, for believing in me before I knew what I wanted or how to get there. I'd like to thank Randy Elble for his exuberant passion for science and his personal investment in my scientific toolbox. Last, I'd like to extend my sincere gratitude to Al Schultz for his enthusiastic support and unending encouragement and to Misha Ugarov and Tom Egan for all their hard work and help in overcoming obstacles along the way.

This work was supported by the National Institutes of Health, the Robert A. Welch Foundation, and Ionwerks, Inc.

TABLE OF CONTENTS

Page

LIST OF FIGURES

FIGURE Page

LIST OF TABLES

TABLE Page

NOMENCLATURE

AAKAA	Ac-(AAKAA)$_n$Y-NH$_2$
AEAAKA	Ac-Y(AEAAKA)$_n$F-NH$_2$
CD	circular dichroism
ε	dielectric constant
ESI	electrospray ionization
IM	ion mobility
MS	mass spectrometry
IM-MS	ion mobility-mass spectrometry
MALDI	matrix-assisted laser desorption ionization
$[M + H]^+$	protonated molecule
$[M + Na]^+$	sodium-coordinated molecule
$[M + X]^+$	alkali metal-coordinated molecules
m/z	mass-to-charge ratio
VT	variable temperature
Ω	collision cross-section

CHAPTER I

BACKGROUND AND INTRODUCTION

Proteins, the workhorses of biological systems, carry out many of the cellular processes required for life (1). Protein structure and function are intimately connected; for example, relatively small structural changes (*e.g.* phosphorylation of a single residue) can result in dramatic functional consequences (*e.g.* activation of a kinase which triggers cell division) (1). Thus, understanding how primary amino acid sequence influences protein folding and structure is paramount to understanding protein function.

The mechanism of protein folding has been the subject of much research and debate (2). If a 100 residue protein randomly searched all possible conformations to find its native state, it would take over 10^{77} years for it to fold (3). However, experimental evidence has shown that protein folding occurs on a short timescale (μs - s) (4). The question then becomes, how do proteins fold? Many hierarchical protein folding theories have been put forth in the literature for soluble proteins (5-8). The framework model or related diffusion-collision model describes protein folding as a process where multiple microdomains (small units of structure) form secondary structures, diffuse and collide to form the native protein structure (5; 6). The nucleation-condensation model differs from the framework, and diffusion-collision, models in that secondary structure is affected by tertiary structure (*i.e.* secondary and tertiary structure form simultaneously (7; 9). In the

---

This dissertation follows the style of the *Biophysical Journal*.

nucleation-condensation model, a folding nucleus forms first and the process continues from the folding center. Gianni and colleagues presented an analysis which highlighted the unified aspects across the hierarchical theories of protein folding whereby the stability of secondary structure determines the mechanism of protein folding (10). For instance, if stable secondary structure is formed first, then the protein would fold by the framework/diffusion-collision model. However, in the absence of any stable secondary structural elements, the protein would likely fold via hydrophobic collapse, where tertiary contacts are formed first, followed by secondary structure (8). Finally, if some secondary structure and tertiary structure form simultaneously (dependently), then the protein would fold via the nucleation-condensation mechanism. Thus, the stability of secondary structural elements may determine the protein folding mechanism.

Determining the relationship between primary structure and the stability of protein secondary structure is fundamental to understanding the mechanism of protein folding. The most common secondary structural element, the α-helix, is stabilized by backbone H-bonds between the amide hydrogen and carbonyl oxygen of (i, i+4, see Figure 1, Right for definition) peptide bonds (4). Because the peptide bond has a permanent dipole (Figure 1, Left), alignment of the carbonyl and amide groups along the helical axis in combination with the dangling (non-H-bonded) carbonyl and amide groups at the termini of the helix results in a helix macrodipole (Figure 1, Right) (11).

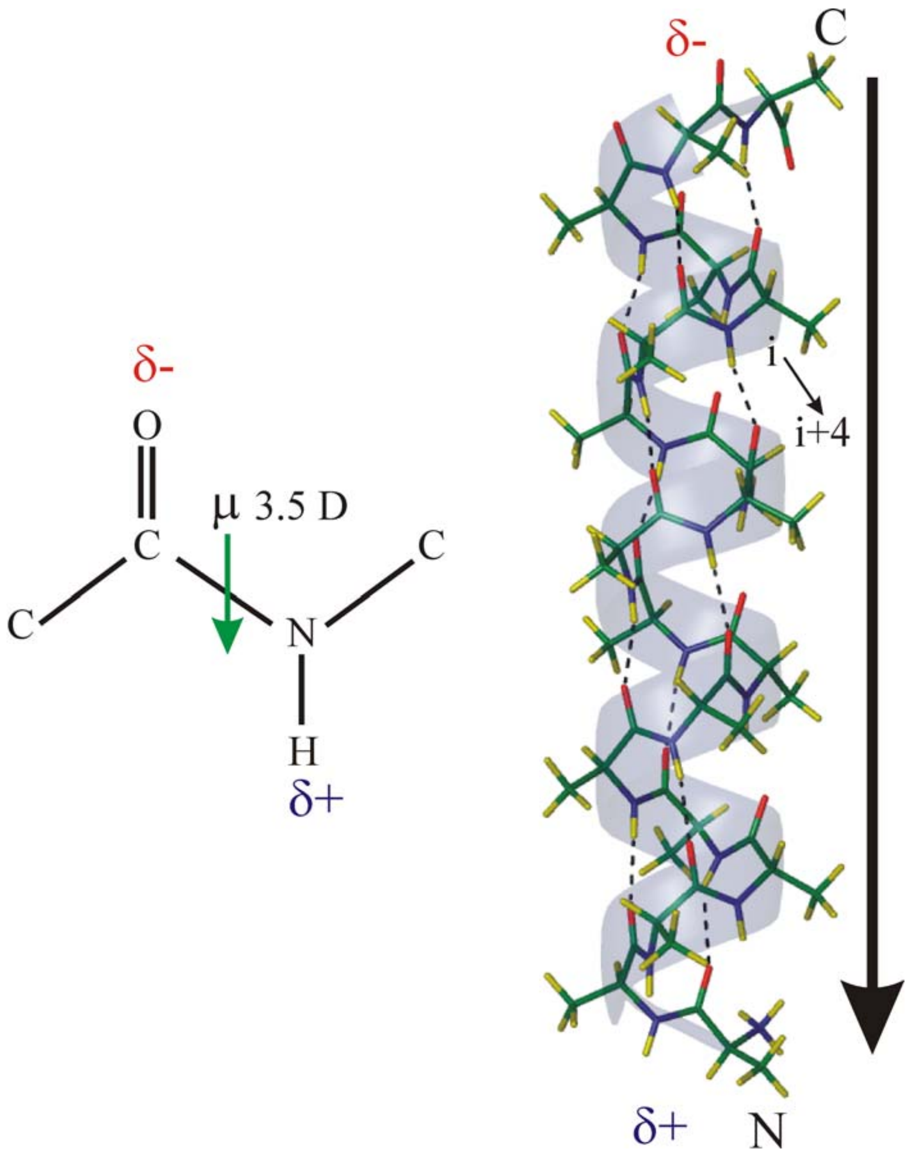

FIGURE 1. Helix macrodipole. (Left) The peptide bond permanent dipole moment (μ) (Right) Polyalanine α-helix in stick and ribbon representation showing alignment of H-bonded carbonyl and amide groups along the helical axis. Adapted from Refs. 11 and 37.

Many groups have tried to relate amino acid composition to helical propensity. Shortly after the first crystal structures became available, a solution-phase helical propensity scale for all 20 amino acids was developed, based on the frequency of occurrence in helical segments in proteins (12). Scheraga and colleagues systematically determined helical propensities for the amino acids using random co-polymers (host-guest studies) (13). Wójcik and co-workers found no substantial difference in helical propensity between the amino acids and suggested that short peptides would not exhibit significant helical structure in solution. Subsequently, peptide systems were developed in the Kallenbach and Baldwin laboratories (14; 15). An experimental helical propensity scale derived by Pace and Scholtz listed amino acid helical propensities in the following order: alanine > leucine > isoleucine > valine >> glycine (16); this helical propensity scale correlates very well with the Chou and Fasman scale and the peptide systems of Kallenbach and Baldwin (14; 15), but not the random co-polymer host-guest studies (13). The reason for the discrepancy between the host-guest and peptide/experimental helix propensity scales is likely due the assumption that the amino acids behave like random co-polymers.

Although solvent plays an important role in determining the stability of helices (17; 18), Pauling and co-workers initially predicted helical peptide folding motifs in the absence of solvent (19). *In vacuo* studies of anhydrous and partially-solvated peptides may provide insight into the role of solvation in protein structure and folding. Furthermore, anhydrous studies allow evaluation of the intrinsic structural propensities of peptides and may shed light on the general protein folding mechanism, *i.e.* (i) determine intrinsic secondary structural stability, (ii) identify autonomous folding units and (iii) evaluate solvent effects on peptide structure.

The coupling of ion mobility (IM) spectrometry, a gas-phase electrophoretic separation, with mass spectrometry (MS), provides a powerful biophysical tool for the study of solvent-free or stepwise-solvated peptide and protein structure (20-22). Analysis using IM-MS results in a two-dimensional correlation between apparent surface area (collision cross-section, Ω) which depends on ion structure and the mass-to-charge ratio (*m/z*) of the ion (Figure 2), allowing detection of multiple conformations of the same *m/z*. Correlation of IM-MS collision cross-sections with model structures generated by simulated annealing allows structural interpretation of the IM-MS data. Gas-phase peptide ions predominately assume a charge-solvated, globular conformation dictated by their gas-phase packing efficiency and define the average, globular peptide mobility-mass correlation (Figure 3) (23-25). However, a small percentage of peptides exhibit intrinsic, gas-phase secondary structure (26-28). Collision cross-sections larger or smaller than those predicted by the globular mobility-mass correlation have been attributed to secondary structure (22; 28-30) or post-translational modification such as phosphorylation or glycosylation (31-33), respectively.

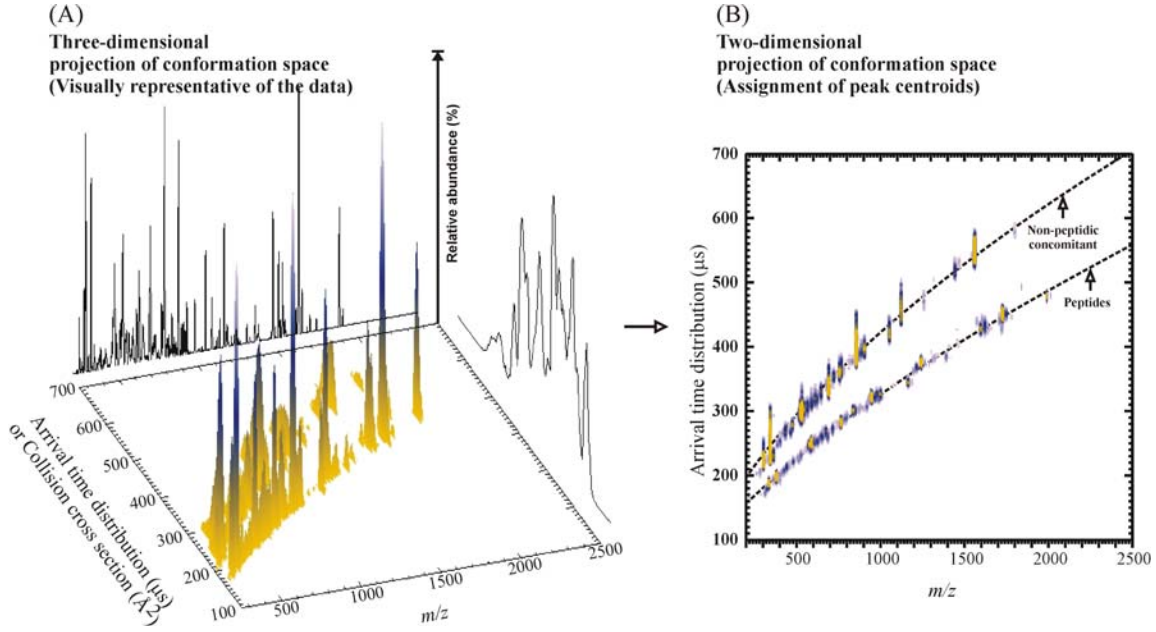

FIGURE 2. IM-MS conformation space (IM arrival time versus *m/z*) projected in (A) 3D and (B) 2D for an *E. coli* cell lysate. The integrated mass spectrum over all conformation space (A, top) is readily deconvoluted into individual mass spectra for peptides and non-peptides (A, right), by integrating regions in conformation space corresponding to their respective structural appearance space.

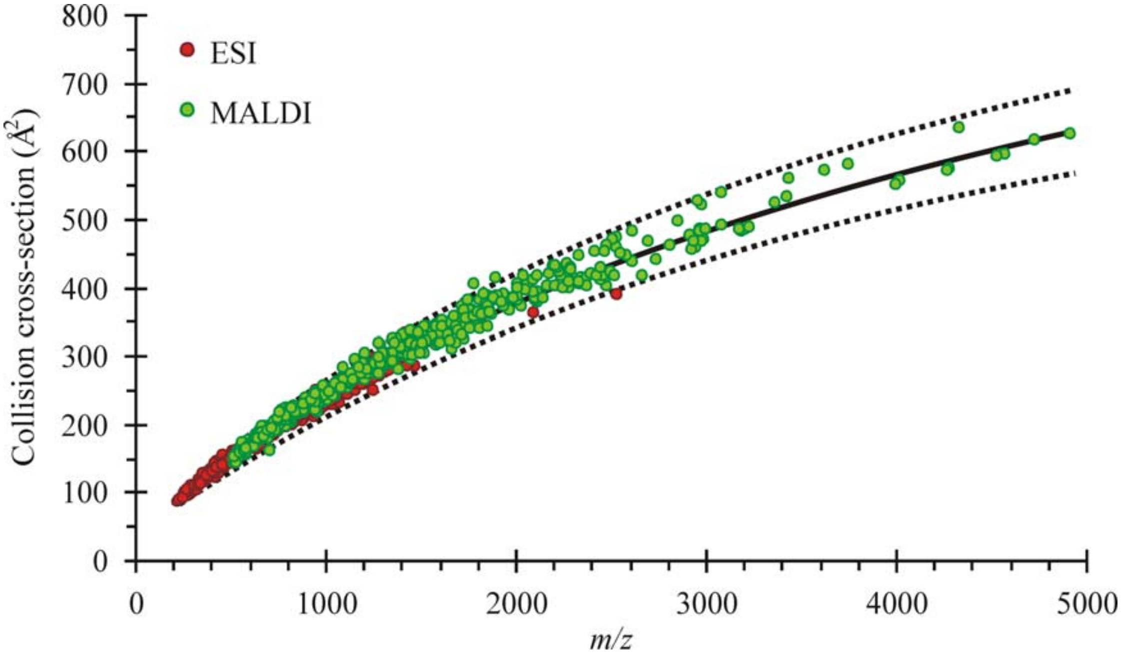

FIGURE 3. Characterization of the average, globular mobility-mass correlation. Collision cross-sections plotted as a function of mass-to-charge ratio for electrospray (ESI) and matrix-assisted laser desorption ionization (MALDI) generated ions of tryptic peptides. The solid line is a third order polynomial fit of the ESI and MALDI data (23; 25; 34). The dotted lines represent ± 10 % of the polynomial function.

In a series of important experiments, Jarrold and co-workers used IM-MS to study polymers of alanine (29; 35), the amino acid with the highest helical propensity in solution (12; 16). They showed that alanine-based peptide ions predominately assume two gas-phase structures—charge-solvated globules and helices (29; 35; 36). In contrast with solution-phase studies, they found that protonated polyalanine ions are not helical in the gas phase unless the N-terminus is blocked by acetylation and a basic amino acid (*e.g.* lysine) is incorporated near the C-terminus. These modifications mitigate unfavorable charge-helix macrodipole (see Figure 1 for description) interactions in low dielectric environments, *i.e.* in vacuum where $\varepsilon = 1$ (37). In addition, acetylation significantly reduces the basicity of the N-terminus, biasing the protonation site toward the C-terminal lysine. Localization of the charge at the C-terminal lysine stabilizes the helix by favorable interaction of the positive charge (proton) with the negative pole of the helix macrodipole (29; 35). Similarly, when a basic residue is placed at the N-terminus of acetylated polyalanine, the helix collapses to form a charge-solvated globule (36). While N- and C-terminal preferences for a subset of amino acids (capping effects) have been noted in proteins and systematically examined in peptides in solution (38-40), electrostatic effects are enhanced in the absence of solvent. Thus, in the low dielectric environment of the mass spectrometer electrostatic effects are strong determinants in gas-phase helix stability.

Following the determination of peptide ion characteristics necessary to promote stable helical structure in gas-phase alanine-based peptides, the Jarrold laboratory began exploring the effect of glycine residue insertion in these systems (41; 42). In solution, glycine has very low helical propensity, due to its conformational flexibility, *i.e.* glycine's side chain, H, does not sterically-hinder peptide backbone rotation, resulting in more conformational degrees of freedom (4; 16). Although, both polyalanine and polyglycine (unmodified) protonated ions adopt charge-solvated globular structures in the gas phase (35), only Ac-polyAK and *not* Ac-polyGK is helical in the gas phase (43; 44). Kaleta and Jarrold inserted blocks of glycine residues into the middle of acetylated alanine peptides with the aim of disrupting helical structure; five or more glycine residues (in a chain length of 15 residues) are required to accomplish this goal (41). It is surprising that so many glycine residues are required to disrupt gas-phase helical structure because a single glycine is considered a helix breaker in solution (45). [Note: Acetylation of the N-terminus of polyalanine is sufficient for helix formation, *i.e.* a C-terminal basic residue is not required, presumably because a backbone carbonyl near the C-terminus becomes the most favorable protonation site (41).] Kaleta and Jarrold conclude that glycine does not act as an entropically-driven helix breaker in the gas phase, but rather glycine insertion affects the relative energies of the globule and helix, resulting in more globular structures (41).

Although simulations and experimental evidence indicate that entropy plays a large role in determining helical structure in solution (46; 47), Kinnear and Jarrold showed that entropy does not determine gas-phase helical structure for small hydrophobic amino acids (48). They determined that gas-phase helical propensity increases from valine >

leucine > alanine (48), which is the opposite of solution-phase trends (12; 16). The likely reasons for the discrepancy between solution and gas-phase are two fold. First, as Kinnear and Jarrold show, the gas-phase packing efficiency of the hydrophobic residues decreases with increasing size which destabilizes the globular state and stabilizes the helical conformation (48). Secondly, the low dielectric of the vacuum severely weakens the hydrophobic effect and decreases the energetic cost of exposing hydrophobic residues on the helical face, whereas, in solution, it is unfavorable to expose hydrophobic residues to solvent (as in the helical conformation).

Kohtani and co-workers showed that alkali metal adduction stabilizes gas-phase helical conformations of polyalanine (49). Molecular models and previous work with protonated polyalanine peptides suggested that the site of the alkali metal coordination was the C-terminus (49), likely because of the dangling carbonyl groups available for metal coordination. Furthermore, as was the case for Ac-polyAK, C-terminal charge location stabilizes helical conformations via favorable interaction of the alkali ion with the helix macrodipole. However, metal coordination results in moderate deformation of the helix near the site of coordination (49). This effect becomes more pronounced when the peptide is coordinated to high charge density divalent metals ions (*e.g.* Ca^{+2}) (50).

In summary, the Jarrold group has laid a strong foundation for gas-phase studies of peptide structure. They have shown that the dominant gas-phase structures of alanine-based peptides are charge-solvated globules (compact, spherical structures) and helices.

They have also established that gas-phase helices are only formed in ions when the charge is located near the C-terminus, due to the favorable interaction of the charge with the helix macrodipole. Furthermore, they have demonstrated that conformational entropy is not the determining factor in gas-phase structure of glycine-containing peptides or the small hydrophobic polyamino acids—polyalanine, polyvaline and polyleucine. Thus the relative abundance of gas-phase globules and/or helices is dependent on amino acid sequence and type of ion species.

Russell and co-workers has contributed to the field of anhydrous peptide ion structure in naturally-occurring peptide sequences (25; 28; 30-32; 51-53). Ruotolo *et al.* discovered a subset of tryptic peptides with significant gas-phase helical propensity (28; 30). In these studies, the helical propensity was influenced by the solvent used in sample preparation, but it is not clear if these solvent effects are reflected in gas-phase structure. The present studies are motivated by these prior studies (28; 30-32; 35; 36) which showed that anhydrous structure is sensitive to charge location, peptide length and sequence as well as the solvent used for MALDI sample preparation.

The solution-phase conformation of the peptides examined here, namely Ac-(AAKAA)$_n$Y-NH$_2$ (n = 3, 4, 5, and 6) and Ac-Y(AEAAKA)$_n$F-NH$_2$ (n = 2, 3, 4, and 5), have been well-characterized by CD and both series exhibit increasing helicity with increasing peptide length (54; 55). In solution, the K and E side chains of the AEAAKA series (i, i+3 spacing) are significantly less helix-stabilizing (by *ca.* 40%) than the optimal spacing (i, i+4) in solution (56; 57), owing to the spatial constraints of the helix which prevent strong side-chain interactions (*i.e.* lysine-glutamic acid H-bonding and/or ion-pairing) in the i, i+3 spacing. The ends of each peptide were originally modified (N-acetylation and C-amidation) in order to minimize unfavorable charge-helix macrodipole interactions because, in solution, the presence of a negative charge at the C-terminus (*i.e.,* COO^-) or positive charge at the N-terminus (*i.e.,* $-NH_3^+$) destabilizes helical conformations owing to unfavorable charge-macrodipole interactions (11; 58). A similar effect is observed for gas-phase ions, *i.e.* protonated polyalanine peptides only form gas-phase helices if the N-terminus is acetylated and a basic site is incorporated at the C-terminus, and thus the use of these model peptides in gas-phase studies is justified (29). Also, by removing the charges at the termini of the peptides, the peptide becomes a better model for a protein segment (*i.e.* the terminal modifications more closely simulate the environment of a peptide sequence in a protein). In the present work, we use the AAKAA and AEAAKA peptide series to investigate the effect of multiple basic and acidic residues (E, K) on gas-phase structure. Our IM-MS results for $[M + H]^+$ and $[M + X]^+$ (X = Li, Na, K, Rb or Cs) species are interpreted using molecular modeling and compared to known solution-phase helical propensities in an effort to better understand the governing principles of gas-phase structure and as a foundation for future step-wise solvation, variable temperature (VT)-IM-MS experiments.

CHAPTER II

METHODS

Sample preparation

The model helical peptides, Ac-(AAKAA)$_n$Y-NH$_2$ (n = 3, 4, 5, 6 and 7) and Ac-Y(AEAAKA)$_n$F-NH$_2$ (n = 2, 3, 4, and 5), were synthesized, lyophilized, and stored at -20 °C (54; 55). Peptide samples were prepared for matrix-assisted laser desorption ionization (MALDI) using the dried droplet method by diluting the peptides (5 mg/ml in H_2O) 1:1 with α-cyano-4-hydroxycinnamic acid (20 mg/ml in methanol) resulting in a 250:1 matrix-to-analyte ratio. Alkali metals in the form of chloride salts were spiked into the MALDI samples to achieve a final concentration of 0.1% (w/v). Our preference for using MALDI for these studies is based on two factors: (1) MALDI yields almost exclusively singly-charged ions, which minimizes structural changes owing to coulombic repulsion associated with high charge state ions (59; 60) and (2) MALDI is a pulsed ionization technique and thus more compatible with IM-MS. Although sample preparation for MALDI requires addition of a large excess of matrix, our previous studies suggest that helical solution-phase structure is not altered by the presence of the matrix (30; 51).

Instrumentation and data acquisition

The MALDI-IM orthogonal time-of-flight mass spectrometer (MALDI-IM-TOFMS, Figure 4) used in these studies was constructed in collaboration with Ionwerks, Inc.

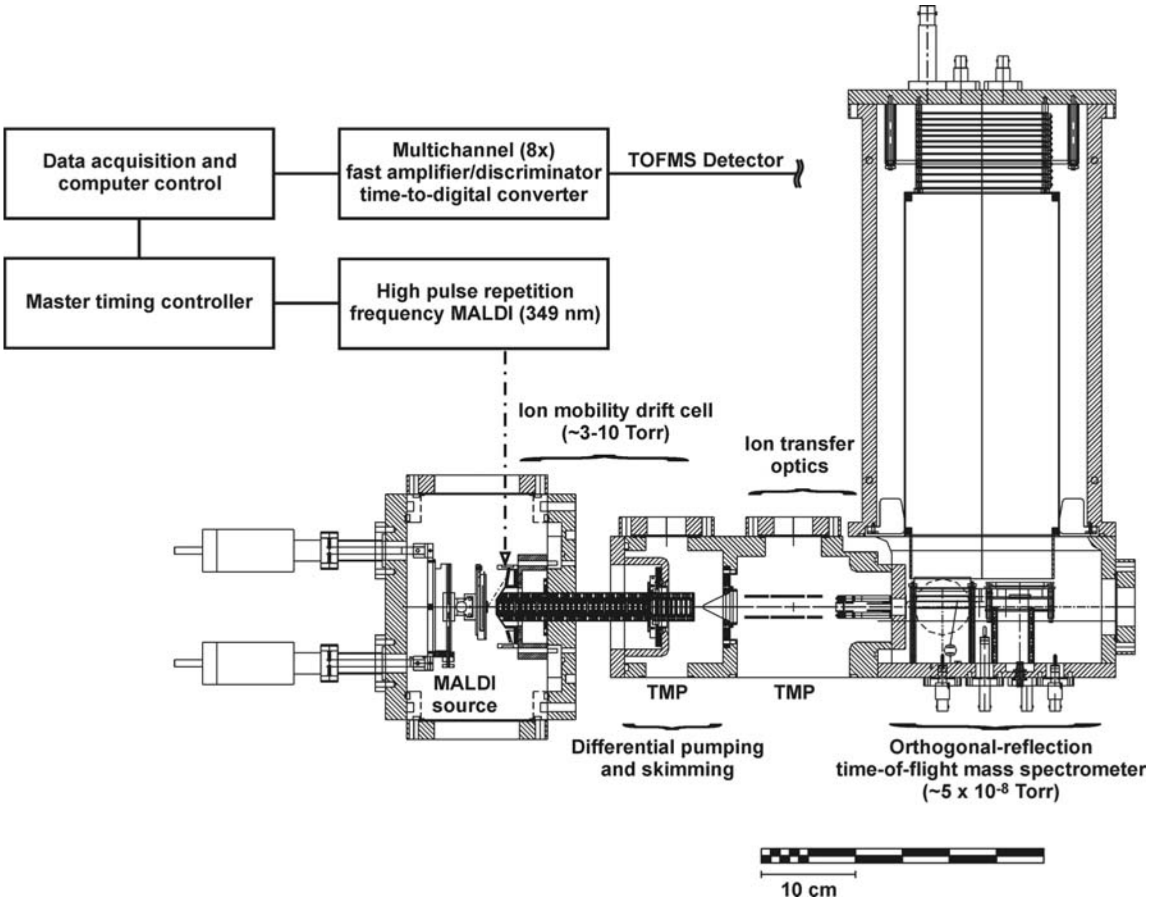

FIGURE 4. Schematic of the MALDI-IM-TOF-MS used in these studies. Ions are generated in the MALDI source and injected into the IM drift cell (maintained at 2-3 Torr He). After the drift cell, the ions are extracted into the source of the TOFMS and mass analyzed. Because the IM drift time (100s of μs – ms) is much longer than for TOF analysis (10s of μs), multiple mass spectra can be acquired during elution from the IM drift cell (*i.e.* multiple mass spectra are acquired over IM profiles).

(Houston, TX) and based on instrumentation previously described by our laboratory (22; 61). MALDI was performed using a frequency-tripled solid state Nd:YLF laser (349 nm, Crystal laser, Reno, NV) operated at a frequency of 300 Hz (62). Singly-charged ions were directed into a 15 cm-long drift cell maintained at approximately 2.5 Torr He (measured with a capacitance manometer (Inficon, Balzers, Liechtenstein)), resulting in IM separation field strengths of 20-50 V cm^{-1} $Torr^{-1}$. All measurements were performed at ambient temperature (*ca.* 297 K). The ion abundances used to generate IM-MS profiles are for the isotope clusters of the specific ion population of interest (*e.g.* $[M + H]^+$, $[M + Na]^+$, etc.). Two-dimensional IM-MS data were acquired and analyzed using custom software (Ionwerks, Inc.).

Collision cross-section calculations

The governing principles of separations by IM are detailed elsewhere (63). Briefly, ions are injected into a drift cell containing a neutral buffer gas and migrate under the influence of a weak electrostatic field. The velocity (v) of the ion is mitigated by collisions with the buffer gas and is related to the electric field strength (E) by a proportionality constant which is the ion mobility (K) in a particular gas:

$$v = KE \qquad (1)$$

$$K = \frac{3q}{16N_o}\left(\frac{1}{m_I}+\frac{1}{m_B}\right)^{\frac{1}{2}}\left(\frac{2\pi}{k_B T}\right)^{\frac{1}{2}}\frac{1}{\Omega} \qquad (2)$$

where mobility is related to the gas number density at STP (N_o), charge of the ion (q, where $q = ze$ and z = charge of the ion, e = elementary charge), mass of the ion (m_I), mass of the buffer gas (m_B), temperature (T), Boltzmann's constant (k_B) and collision cross-section of the ion-neutral pair (Ω) (64). It is conventional practice to report the reduced mobility (K) which normalizes the mobility to STP for comparing measurements conducted at different pressures (P) and temperatures (T):

$$K_0 = K\left(\frac{P}{P_0}\right)\left(\frac{T_0}{T}\right) \tag{3}$$

By substitution and rearrangement of Eqns. 1-3, the empirical collision cross-section is determined by the relation (63):

$$\Omega = \frac{(18\pi)^{1/2}}{16}\frac{ze}{(k_bT)^{1/2}}\left(\frac{1}{m_I}+\frac{1}{m_B}\right)^{1/2}\frac{t_dE}{L}\frac{760}{P}\frac{T}{273.15}\frac{1}{N_0} \tag{4}$$

where t_d is the transit time of the ion in a drift cell of length L and the other parameters are as defined above. Eq. 4 is only valid within the "low field limit" (when the following inequality is satisfied) (64):

$$\left(\frac{m_I}{m_B}+\frac{m_B}{m_I}\right)eE\lambda << kT \tag{5}$$

where λ is the ion mean free path. In this limit, the energy acquired by the ions due to the electric field (field energy) is negligible compared with thermal energy and the separation is within the "low field limit" (Figure 5). That is, the ion energy gained due to the electrostatic potential across the drift cell is dissipated by cooling collisions with the buffer gas (*i.e.* the ions are thermalized). It follows that the experimental metric used to describe the energy of an ion during IM separation is a function of the electric field strength and the number density or pressure of the buffer gas—E/N_o or E/p (64). All IM-

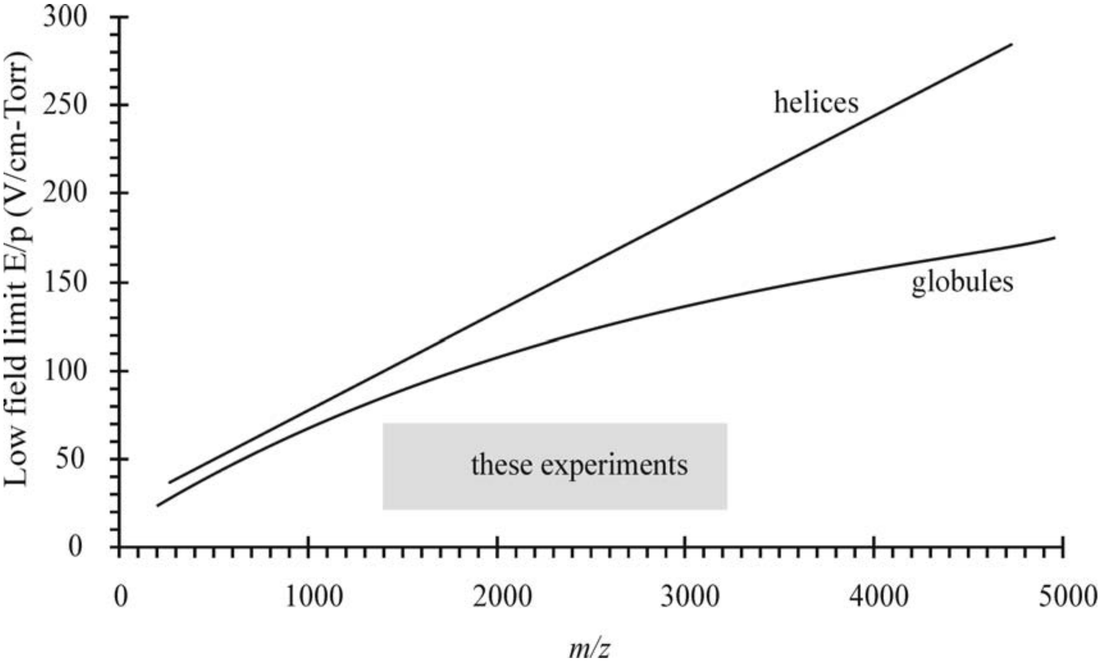

FIGURE 5. The low field limit for globules (lower curve) and helices (upper curve) over a range of m/z values. The low field limit was calculated from Eq. 5. Note: The field energy is expressed as *E/p* (V/cm-Torr) and can be converted to E/N_o (10^{-17} V-cm^2) by multiplying by 4.03 (T = 298K) (63). The globular collision cross-sections were derived from the average mobility-mass correlation (as described in Figure 3) and the α-helical collision cross-sections were calculated using MOBCAL (65) for rigid helices of the same amino acid sequence.

MS spectra were acquired under “low-field” conditions (63; 64; 66). Spectra were obtained at five IM voltages to accurately estimate the mass-dependent drift time correction, t_o ($t_{measured} - t_o = t_d$), which represents the time that the ion spends outside of the IM drift cell. The mass-dependent drift time correction was obtained as the y-intercept of a linear regression of arrival time versus 1/V, where V is the potential across the drift cell (Figure 6).

It is important to note that significantly different drift-time distributions (peak widths) are observed for different ion populations. IM peak broadening, which is dominated by diffusion of the ions in the buffer gas as they traverse the drift cell, can be modeled using classical diffusion and flux equations (63; 67). We modeled peak profiles for an ion population composed of a *single* collision cross-section using Monte Carlo simulations of ion electrodynamics (68). Furthermore, we used predicted peak width values in conjunction with peak deconvolution techniques (53) to estimate the range of structural diversity for a given ion population, *i.e.* to estimate the number of un-resolved populations.

Injected ion studies were performed by incrementally increasing the potential between the sample plate and the entrance to the drift cell, similar to those reported previously (69). The injected ion potential increases the kinetic energy of the ion, resulting in energetic collisions (collisional heating) and subsequent annealing of ion structure prior to IM structural analysis in the drift cell.

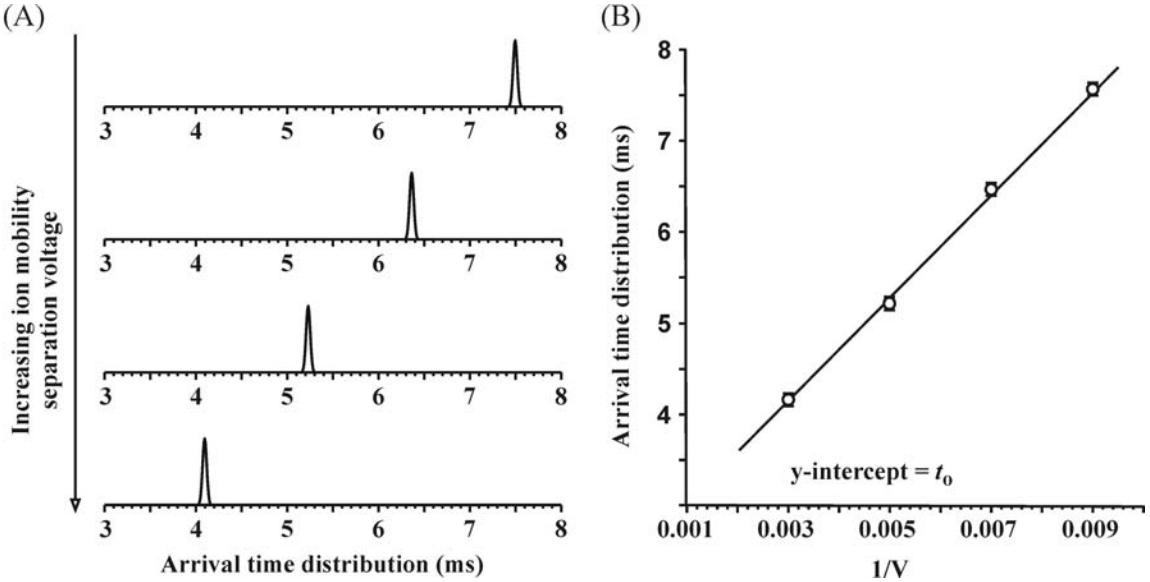

FIGURE 6. Drift time correction procedure. (A) IM-MS spectra are obtained over a series of IM voltages (B) Measured ion arrival times are plotted as a function of the inverse IM voltage (1/V) to accurately estimate the mass-dependent drift time correction, t_o ($t_{measured} - t_o = t_d$), which is the y-intercept of a linear fit to the data points.

Definition of helical content

Helical content is defined by Eq. 6:

$$\text{Helical content (\%)} = I\left(\frac{\Omega_{\text{obs}} - \Omega_{\text{glob}}}{\Omega_{\text{helix}} - \Omega_{\text{glob}}}\right) \text{x } 100 \qquad (6)$$

In cases where the IM profile is bimodal, *I* values correspond to the relative abundance of the integrated peak area of the larger collision cross-section and Ω_{obs} is that determined at the maximum of the larger peak profile. In cases where the profile is dominated by a single peak (I = 1), Ω_{obs} is that determined at the maximum of the peak profile. Ω_{glob} is the predicted collision cross-section for charge-solvated globules derived from the mobility-mass correlation (a third-order polynomial fit to a dataset of collision cross-sections (23; 34)) and Ω_{helix} is the calculated collision cross-section for a rigid α-helix. We assume that any positive deviation from the average mobility-mass correlation is a result of helical structure. Conversion of the measured collision cross-sections to helical content (Eq. 6) normalizes the dataset for both relative abundance of the extended population and the mass-dependent relative difference between globular and helical collision cross-sections, allowing us to examine structural trends as a function of peptide length.

Molecular modeling

Theoretical peptide structures were generated using simulated annealing as previously described (28). *In silico* models were generated using Insight II v2000.2 (70) and simulated annealing was performed using Cerius^2 v4.9 (71). Simulations were performed from multiple starting structures to sample peptide conformational space. Initially, simulations were started from two conformations: α-helical and fully extended. Because the gas-phase basicity of lysine is approximately 16 kcal/mol higher in energy than the carboxamide C-terminus, (72) only lysine residues were considered as charge carrying sites in the simulations. Protons were covalently attached to the lysine side chain for both peptide conformations; this resulted in $2n$ starting conformations (n = the number of repeats or lysines) per ion. The final structure from each annealing cycle was minimized, generating 300 structures per trajectory. The total simulation time for each simulated annealing run was 2.5 ns (dielectric = 1, 300 annealing cycles, time step of 1 fs, temperature range = 300 – 1000 K with temperature increment of 50 K and a relaxation time of 0.1 ps using the T-damping thermostat (73), see Figure 7 for a graphical representation of temperature changes over a single cycle). All simulations were performed using the Open Force Field (OFF) force field driver and the Consistent Force Field (CFF) v1.02 as implemented in Cerius2 v4.9 (71). In total, $600n$ (1200-3600 for n = 2-6 respectively) candidate structures were generated for each species in this first tier of modeling. A second tier of simulated annealing was performed by starting simulations from 5-10 of the lowest energy conformations of the first tier of modeling. All molecular modeling images were generated using Insight II v2000.2 (70) or Pymol (74).

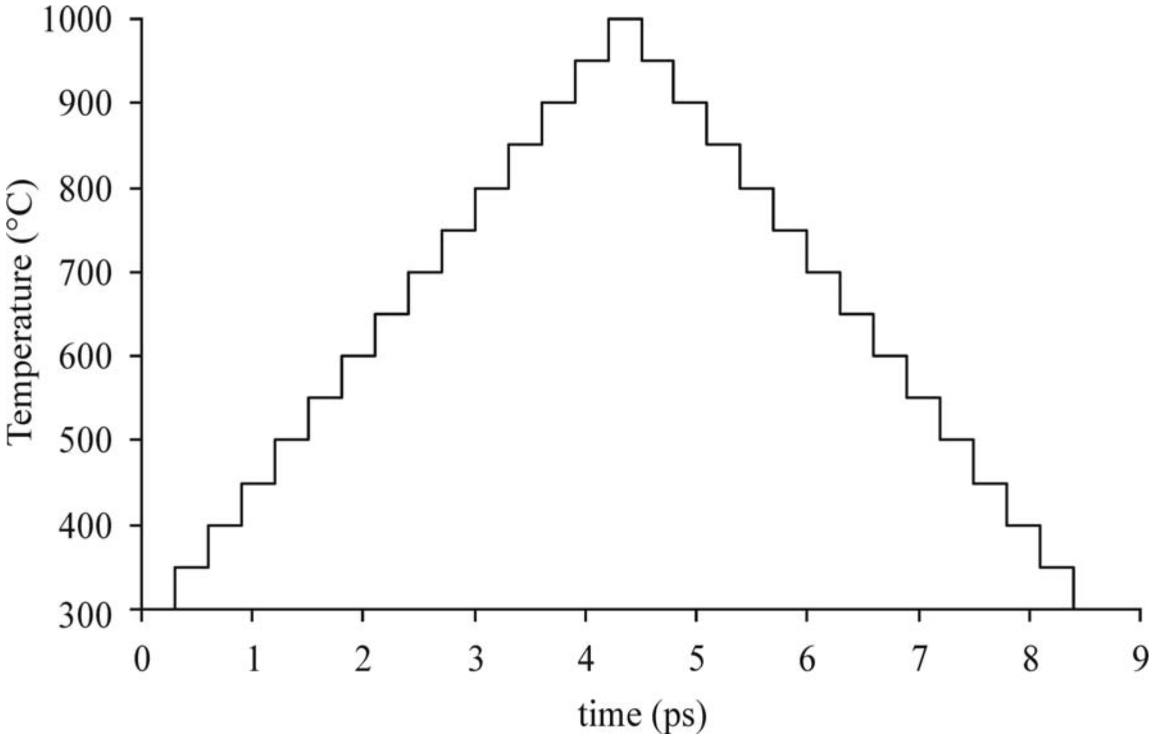

FIGURE 7. Protocol used for a single cycle of simulated annealing. 8.4 ps simulation time/cycle, temperature range = 300 – 1000 K. 300 cycles of annealing were completed per annealing trajectory, generating 300 ion structures.

The collision cross-sections of all models were calculated using the trajectory method in MOBCAL (65). The potential energy for each model structure (from molecular dynamics) was plotted versus the calculated collision cross-sections to visualize the spread in energy and collision cross-section of all structures generated for a particular species (Figure 8). For comparison with empirical IM-MS results, simulation collision cross-sections within 2% were found for most ions (gray bar in Figure 8). However, there were few compact structures in these initial simulations. We surmised that this was due to an underestimation of non-bonding interactions.

More computationally-intensive molecular modeling studies with increased non-bonding interaction distances (30 Å nonbonding cutoff vs. 8 Å nonbonding cutoff in the methods described above) were performed for all metal-coordinated ions and $[M + H]^+$ of AAKAA $n = 6$ and 7 in order to better sample peptide conformations with extensive intramolecular contacts (*e.g.* compact conformations, see Figure 8 for graphical representation). All other simulation parameters were maintained as above. All results shown for $[M + H]^+$ ions have an 8 Å cutoff except for AAKAA $n = 6$ and 7 which have a 30 Å cutoff. All results shown for metal-coordinated ions have a 30 Å cutoff.

The secondary structural elements present in each model structure were characterized using Kabsch-Sander definitions implemented in Insight II v2000.2 (75). The percentage of each element (helix (α, π and 3/10), β-sheet, or turn) is reported by

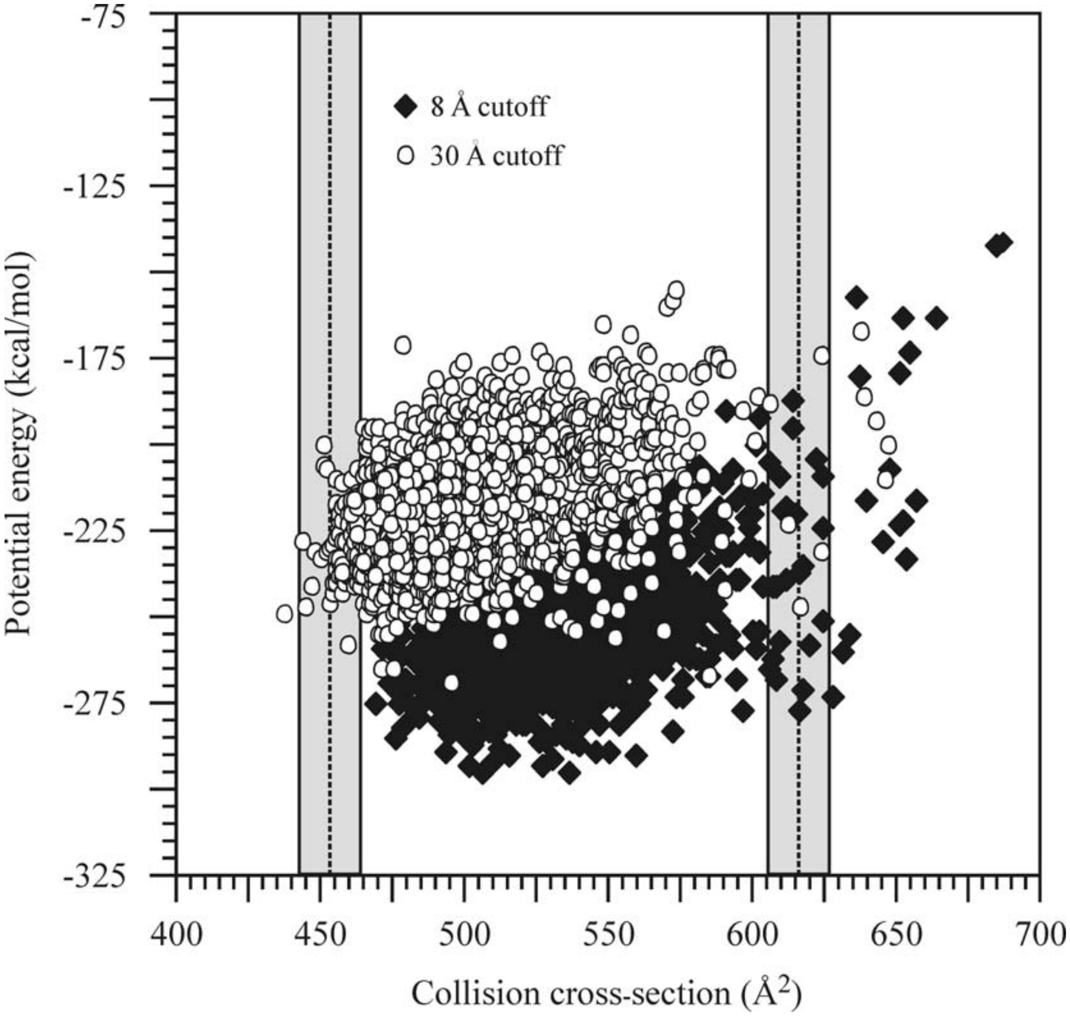

FIGURE 8. Cluster plot of molecular dynamics energy versus calculated collision cross-sections for two nonbonding cutoffs (8 Å and 30 Å) for $[M + Na]^+$ ions of Ac-Y(AEAAKA)$_4$F-NH$_2$. The dotted lines are the measured collision cross-sections obtained by IM-MS and the gray bars represent ± 2 % of these values (the precision of our IM-MS measurements).

dividing the number of residues exhibiting secondary structure by the total number of residues

The helical mobility-mass correlations for ideal α-, π− and 3/10- helices for the AEAAKA and AAKAA peptide ions were estimated by generating energy minimized model structures in Insight II v2000.2 (70)and calculating their collision cross-sections using MOBCAL (65).

CHAPTER III

ANHYDROUS STRUCTURE OF PROTONATED PEPTIDES

Introduction

Over the past decade the potential of structural mass spectrometry techniques for studies of gas-phase biomolecular ions and complexes of biomolecular ions have evolved, and advances in computational techniques for large molecules have greatly enhanced our ability to infer structure from mass spectrometry data. Ion mobility-mass spectrometry (IM-MS), a gas-phase electrophoretic separation technique coupled to a modern mass spectrometer (76), represents another powerful biophysical tool to study solvent-free or stepwise-solvated peptide and protein ion structure (20-22; 28; 30; 77). Although ion mobility spectrometry has been extensively used for studies of fundamental ion chemistry, only recently has its utility for biological studies been realized (26; 59). The importance of IM-MS as a biophysical tool is the ability to correlate empirical collision cross-sections (apparent surface area) and accurate mass-to-charge measurements (*m/z, i.e.* molecular weight) to candidate structures derived using molecular dynamics and molecular orbital calculations (29; 59; 78; 79). The inherent advantages of IM-MS as a structural mass spectrometry tool are further enhanced by variable-temperature (VT) IM-MS to determine thermo-chemical data for interconversion between different structural forms (42).

Previous studies have shown that most gas-phase peptide ions adopt compact, globular conformations dictated by their intrinsic gas-phase packing efficiencies, defining an average globular peptide mobility-mass correlation (23; 24; 80). Conversely, some peptide ions exhibit ordered structure in the gas phase (26; 27), yielding collision cross-sections that are either larger or smaller than those predicted by globular peptide mobility-mass correlation (22; 28-30; 35). Elongated, helical structures yield larger collision cross-sections, whereas intramolecular interactions between polar residues, *i.e.,* formation of salt-bridges and post-translational modifications yield smaller than predicted collision cross-sections (22; 31; 32).

Helices are the most common secondary structural element of transmembrane proteins (81), thus the forces that dictate the formation and stability of helices are fundamental to understanding protein folding. On the other hand, much of our understanding of protein folding is based on experiments performed in aqueous solutions and we have very limited understanding of the effects of low dielectric environments and/or non-polar solvents (82; 83). Nonetheless, the potential importance of solvent-free peptide structure studies is underscored by Pauling's prediction of helical peptide folding motifs in the absence of solvent (19).

A strong foundation for studying gas-phase helices exists based on the work of Jarrold and co-workers who used IM-MS to study gas-phase polyalanine ions (29; 35; 36; 78; 79), which exhibit high helical content in aqueous solution (12; 16; 57); however, they found that $[M + H]^+$ polyalanine ions adopt helical conformations only if the charge is localized near the C-terminus (*i.e.* by blocking the N-terminus by acetylation and introducing a basic residue near the C-terminus), which stabilizes the helix by favorable interactions of the positive charge with the helix macrodipole (29; 35). Russell and co-workers previously reported data for a subset of tryptic peptides with significant helical structure (28; 30), and showed that the same peptides exhibit helical preferences in solution (as measured by circular dichroism (CD)). Furthermore, a good correlation between results obtained by CD and H/D exchange was demonstrated (30). The present work builds upon these earlier studies and is aimed at understanding how amino acid sequence affects anhydrous structure in peptides that contain multiple acidic and/or basic residues.

The solution-phase conformation of the peptides Ac-$(AAKAA)_n$Y-NH_2, n = 3, 4, 5, 6 and 7, and Ac-Y$(AEAAKA)_n$F-NH_2, n = 2, 3, 4, and 5, has been well-characterized by CD. Both series exhibit increasing helicity with increasing peptide length (54; 55). Here, we examine the relationship between helical content, primary sequence and peptide length in the AAKAA and AEAAKA series. Previously, Jarrold showed that insertion of an E/K pair into Ac-$A_3G_{12}K$ decreased the helical content of the anhydrous peptide ions compared to the unsubstituted peptide (84). In the present work, we use the AEAAKA peptide series to investigate the effect of multiple E/K pairs on gas-phase structure and compare the helical content of this peptide series to that of the AAKAA series to provide a foundation for future studies of step-wise solvation and VT-IM-MS experiments.

Results and discussion

The model peptides Ac-(AAKAA)$_n$Y-NH_2 and Ac-Y(AEAAKA)$_n$F-NH_2, hereafter simply referred to as AAKAA and AEAAKA, respectively, are used to probe the effects of peptide length, primary sequence, and number of basic (K) and acidic (E) residues on gas-phase ion structure. The AAKAA and AEAAKA model peptides were originally designed in the R. L. Baldwin laboratory to study the effect of peptide length on solution-phase helical content (54; 55); these studies showed that the helical content of the AEAAKA and AAKAA peptides increases with peptide length. For the purposes of our gas-phase studies, we assume that differences in the N- and C-terminal residues of the AAKAA (C-terminal Y) and AEAAKA (N-terminal Y; C-terminal F) do not affect the charge site of the ion and therefore have no significant impact on gas-phase structural trends. That is, the site of protonation should be a K residue. The presence of a negative charge at the C-terminus (*i.e.,* COO^-) or positive charge at the N-terminus (*i.e.,* -NH_3^+) destabilizes helical conformations owing to unfavorable charge-macrodipole interactions (58); therefore the ends of the AAKAA and AEAAKA peptides were originally modified (N-acetylation and C-amidation) in order to minimize unfavorable charge-helix macrodipole interactions in solution (11). Similarly, gas-phase protonated polyalanine peptides only form gas-phase helices if the N-terminus is acetylated and a basic site is incorporated at the C-terminus, justifying the use of these AAKAA and AEAAKA peptides in the present gas-phase studies (29).

Figure 9 contains IM-MS data plotted as abundance of $[M + H]^+$ ions versus IM drift time (t_d, upper axes) and collision cross-section (Ω, lower axes) for the AAKAA (n = 3 - 7) peptide series. The dashed vertical lines in Figure 9 represent the average peptide mobility-mass correlation (derived from a third order polynomial fit of a dataset of 964 $[M + H]^+$ peptide ions (23; 34)) for charge-solvated, globular peptide ions and the solid vertical lines represent the calculated collision cross-sections for rigid α-helical conformations. Note that the absolute difference in collision cross-section between globular and helical structures increases as peptide length increases because helix propagation impacts the collision cross-section more per amino acid due to the aspect ratio of a helix (approximated by a cylinder) compared to a globule (approximated by a sphere) (85).

The IM profiles for the $[M + H]^+$ ions of the AAKAA series are each composed of a single peak, centered at a collision cross-section that falls between the expected values for globules and helices (Figure 9). As AAKAA peptide length increases, the relative abundance of the more compact (globular) structures increases. This is especially apparent for the longest AAKAA peptides (n = 6 and 7), which exhibit bimodal distributions. The structures that correlate with the measured collision cross-sections for the $[M + H]^+$ ions of AAKAA n = 3 - 5 correspond to partial helices (Figure 10). For

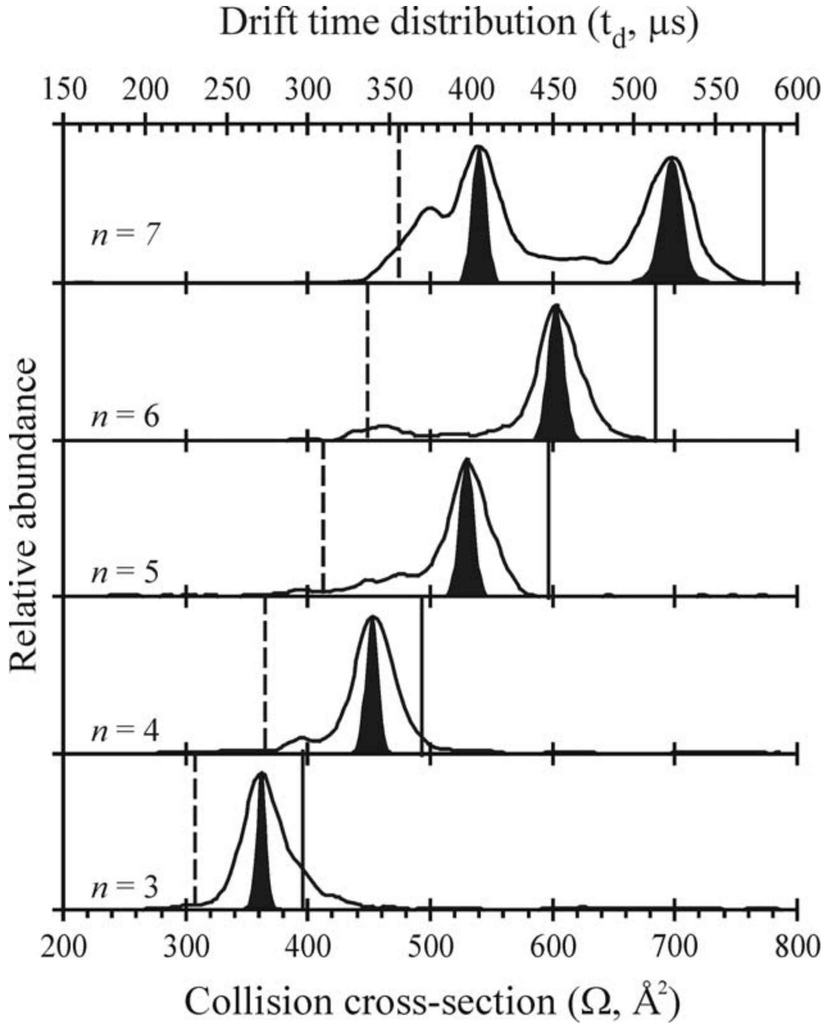

FIGURE 9. Ion mobility drift time (upper x-axis) and collision cross-section (lower x-axis) profiles for $[M + H]^+$ ions of Ac-(AAKAA)$_n$Y-NH$_2$ (n = 3, 4, 5, 6 and 7). The dashed vertical lines represent the predicted collision cross-sections for globular peptide mobility-mass correlation (as defined in Figure 3) and the solid vertical lines represent the α-helical mobility-mass correlation (calculated collision cross-sections for α-helices of the same amino acid sequence). The shaded profiles are simulated IM profiles for a single collision cross-section, assuming peak broadening is solely due to longitudinal diffusion.

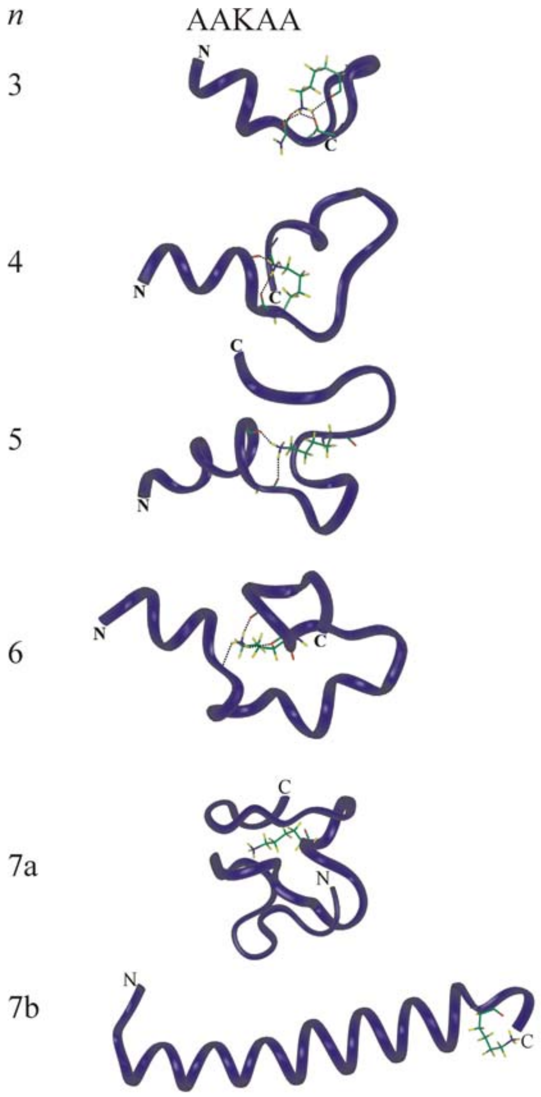

FIGURE 10. The lowest energy structures generated using molecular dynamics for compact and extended conformations of $[M + H]^+$ ions for Ac-(AAKAA)$_n$Y-NH$_2$ (n = 3, 4, 5, 6 and 7). '7a' and '7b' correspond to the compact and extended conformations for n = 7, respectively. "N" and "C" indicate the N- and C-termini, respectively. The protonated lysine side chains and all atoms H-bonded to the proton are shown in cylinder representation.

n = 6 and 7, the ions with bimodal distributions, the peak profile on the left (shorter drift time) correspond to charge-solvated globules and the peaks profiles on the right (longer drift time) correspond to partial helices. The globular IM profile for *n* = 7 appears to contain at least two subpopulations as evidenced by the shoulder on the profile biased towards smaller collision cross-sections. Notice that there is significant bridging in the IM profile for *n* = 7 between the globule and distorted helix, indicating structural interconversion on the timescale of the experiment (< 1 ms).

One important issue to address is approximately how many structural populations are represented by the experimental peak widths for the AAKAA ions. Using simulations developed by Raznikov and co-workers, peak profiles were estimated for ion populations where peak broadening arises exclusively from ion diffusion (68). That is, we expect the simulated peak widths to approximate the experimental profiles if the empirical profile is the result of structures corresponding to a single collision cross-section, *i.e*. an ensemble of closely-related structures. The shaded peaks (Figure 9) are the simulated peak profiles and clearly show that the experimental profiles are broader than the simulated profile, indicating that there are a few, related structures which remain unresolved for the AAKAA $[M + H]^+$ ions.

Very different drift-time distributions (Figure 11) are observed for AEAAKA $[M + H]^+$ ions. With the exception of *n* = 2, all AEAAKA $[M + H]^+$ ions exhibit a single IM peak that correlates with globular conformations (dashed line) and structures that match the

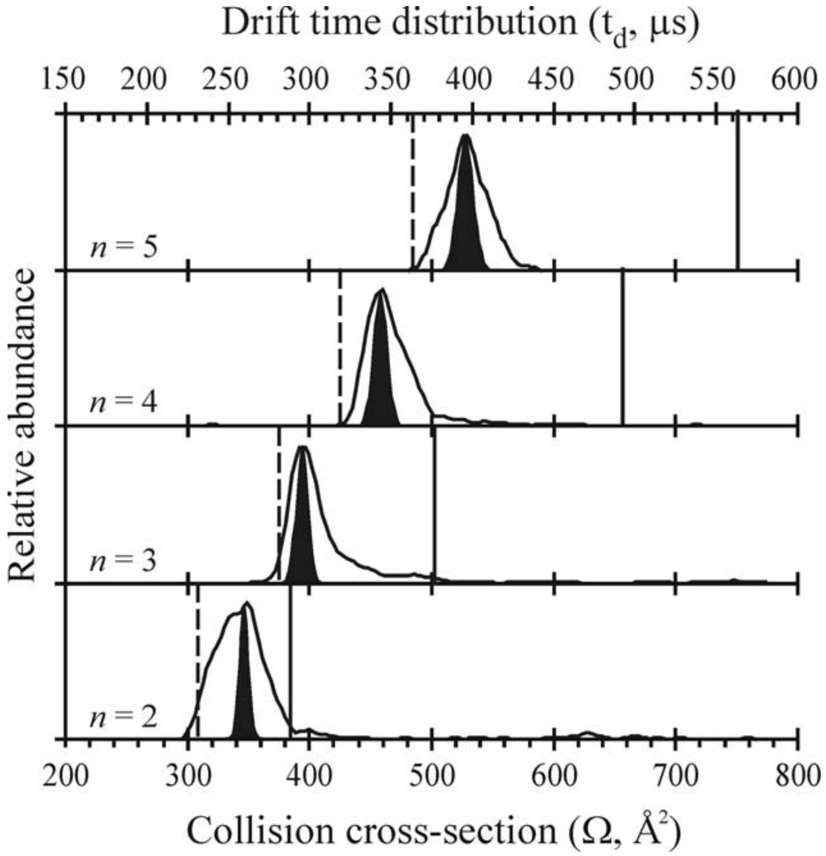

FIGURE 11. Ion mobility drift time (upper x-axis) and collision cross-section (lower x-axis) profiles for $[M + H]^+$ ions of Ac-Y(AEAAKA)$_n$F-NH$_2$ (n = 2, 3, 4, and 5). The dashed vertical lines represent the predicted collision cross-sections for globular peptide mobility-mass correlation (as defined in Figure 3) and the solid vertical lines represent the α-helical mobility-mass correlation (calculated collision cross-sections for α-helices of the same amino acid sequence). The shaded profiles are simulated IM profiles for a single collision cross-section, assuming peak broadening is solely due to longitudinal diffusion.

measured collision cross-sections are charge-solvated globules (Figure 12). For the *n* = 2 ion, the experimental peak profile is very broad compared to the simulated peak profile (Figure 11, shaded profile). Structures which match the average collision cross-section for *n* = 2 are best described as partial or distorted helices (Figure 12), though it is possible that the ions are interconverting between globule and helix on the timescale of the experiment.

It is interesting to compare data for AAKAA peptides to that of the AEAAKA series. The $[M + H]^+$ collision cross-sections plotted as a function of *m/z* provide an overview of the structural trends across both series (Figure 13, see Table 1 for list of collision cross-section values). Both of the short peptides (AAKAA, *n* = 3 and AEAAKA, *n* = 2) exhibit collision cross-sections intermediate between globules and helices. The longer AAKAA ion signals also fall between globules and helices, but a charge-solvated globular population grows in as peptide length (and number of basic sites) increases. The longer AEAAKA ions exhibit collision cross-sections indicative of globules.

To normalize for the absolute difference in collision cross-section between globules and helices as m/z increases, we calculated helical content (Eq. 6, Figure 14), a metric similar in concept to the "relative collision cross-sections" reported by Hudgins and co-workers (36): the major difference is that helical content accounts for the relative abundance of the helical population (for bimodal distributions). The helical content remains relatively constant (ca. 60%) for AAKAA n = 3 - 5 $[M + H]^+$ ions, but then

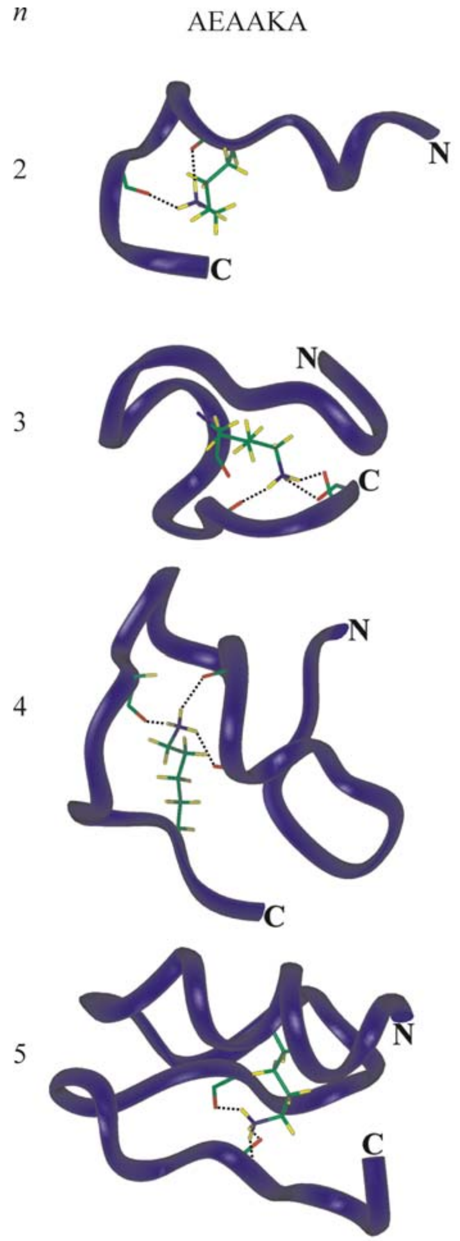

FIGURE 12. The lowest energy structures generated using molecular dynamics for $[M + H]^+$ ions for Ac-Y(AEAAKA)$_n$F-NH_2 (n = 2, 3, 4, and 5). "N" and "C" indicate the N- and C-termini, respectively. The protonated lysine side chains and all atoms H-bonded to the proton are shown in cylinder representation. The dashed black lines represent H-bonds.

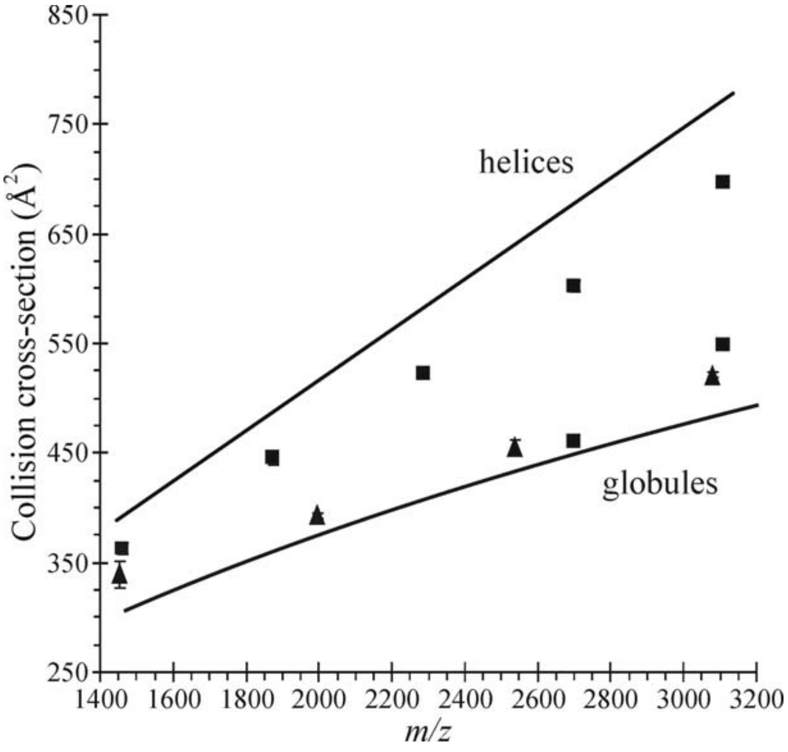

FIGURE 13. Plot of collision cross-section versus m/z for $[M + H]^+$ ions for AAKAA (■) and AEAAKA (▲). The solid lines represent the mobility-mass correlations for globular and helical peptide ions as defined in Figure 3. Error bars represent ±1 σ for 10 measurements. For clarity, error bars are not shown for the globular or helical mobility-mass correlations.

TABLE 1. Mass-to-charge ratios (*m/z*), collision cross-sections (Ω) and reduced mobilities (K_o) for $[M+H]^+$ ions for Ac-(AAKAA)$_n$Y-NH$_2$ (*n* = 3, 4, 5, 6 and 7) and Ac-Y(AEAAKA)$_n$F-NH$_2$ (*n* = 2, 3, 4, and 5) where *n* = the number of peptide repeats and subscripts indicate compact (c) or extended (e) conformations. Mass-to-charge values were calculated using average masses. Collision cross-sections and reduced mobilities are reported as the average ± 1σ for m measurements.

	n	species	m/z	Ω (Å^2)	K_o	m
Ac-(AAKAA)$_n$Y-NH$_2$	3	$[M+H]^+$	1460.72	362 ± 5	1.486 ± 0.020	10
	4	$[M+H]^+$	1873.21	446 ± 6	1.207 ± 0.018	10
	5	$[M+H]^+$	2285.70	522 ± 4	1.030 ± 0.009	10
	6	$[M+H]^+_c$	2698.19	486 ± 16	1.142 ± 0.009	17
		$[M+H]^+_e$	2698.19	609 ± 20	0.908 ± 0.005	27
	7	$[M+H]^+_c$	3110.68	549 ± 21	1.019 ± 0.012	17
		$[M+H]^+_e$	3110.68	697 ± 26	0.802 ± 0.004	17
Ac-Y(AEAAKA)$_n$F-NH$_2$	2	$[M+H]^+$	1453.64	339 ± 12	1.590 ± 0.056	10
	3	$[M+H]^+$	1995.24	393 ± 3	1.370 ± 0.009	10
	4	$[M+H]^+$	2536.85	456 ± 6	1.181 ± 0.016	10
	5	$[M+H]^+$	3078.45	521 ± 3	1.032 ± 0.006	10

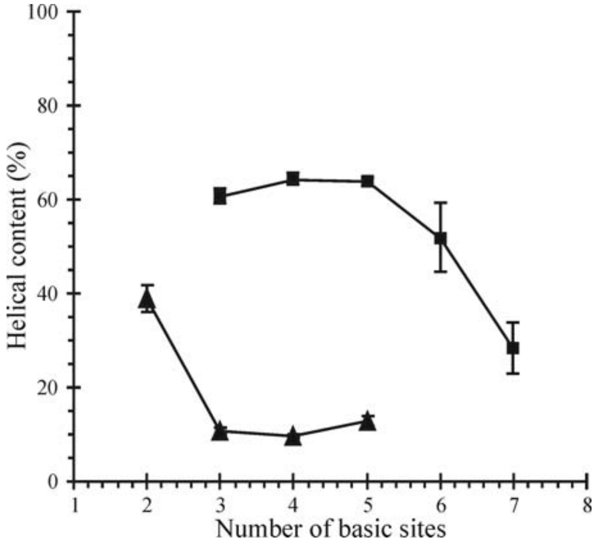

FIGURE 14. Plot of helical content vs. number of basic amino acid residues for the AAKAA (■) and AEAAKA (▲) $[M + H]^+$ peptide ions. The helical content is defined in Eq. 6. Error bars represent ±1 σ for 10 measurements.

decreases for the longest AAKAA peptides. Helical content decreases with peptide length for AEAAKA $[M + H]^+$ ions as well, but the onset occurs with fewer basic sites than for the AAKAA peptides, with only the $n = 2$ ion exhibiting appreciable helical content.

To probe the thermodynamic stability of ion structural populations, we used ion injection techniques similar to those reported elsewhere (69). Briefly, this methodology consists of accelerating the ion population, from the point of ion generation, so that the ions experience *ca.* 10-100 higher energy collisions (*i.e.* the ions are collisionally-heated). The ions are then cooled by collisions with the buffer gas and injected into the IM drift cell for structural analysis. If the ions comprising a particular population are easily converted to another structure (*i.e.* helix → globule), then we expect to observe changes in the relative peak areas for a particular conformation as a function of the ion injection voltage.

In the ion injection studies presented here, the ion temperature increase over the system temperature (297 K) owing to the initial higher energy collisions (100 eV lab frame energy), is estimated to range from *ca.* 5 to 28 K for the largest ($n = 6$) to the smallest ($n = 3$) injected ion species, respectively. These estimates are based on calculations derived from kinetic theory, and represent an upper limit of temperature. Thus, even in this limit, the ion temperature likely remains well below *ca.* 350-400 K, after which the ions are collisionally-cooled prior to injection into the drift cell. This premise is further supported by the absence of *b*-type ions arising from increased injection energy (data not shown). This ion class (*b*-type) is indicative of thermally-activated dissociation of helices (86).

Injected ion experiments for short AAKAA peptides (*n* = 3 – 5) revealed no apparent change in ion structure (Figure 15A). However, long AAKAA peptides exhibit dramatic structural changes when heated. Injected ion studies of AAKAA *n* = 6 (Figure 15B) show a structural conversion from partial helix to globule as the injection potential increases. The IM profile for the 100 V potential (top panel) is bimodal with significant bridging between the globule and partial helix populations, suggesting that the ions are interconverting on the timescale of the experiment. Extensive analysis of this profile reveals many possible structural sub-populations that are unresolved within the broad profile (Figure 16). Each peak under the experimental profile represents a simulated peak with a width expected for a single collision cross-section. Previous results from the Jarrold laboratory have shown that C-terminal charge location is the dominant factor in gas-phase helix stabilization (29; 79). Thus, it is likely that the proton becomes mobile in the heated AAKAA *n* = 6 ion because both compact (N-terminal localization), intermediate, and extended conformations (C-terminal localization) are observed. Heating of the longest AAKAA ion (*n* = 7) by increasing the field strength (see Methods, Chapter II) also elicits a dramatic structural re-organization (Figure 17). In this case, the ion structure transitions from a tightly-packed globule (A) to an expanded globule (B) to a partial helix (C) with increasing separation field strength. Inset in the

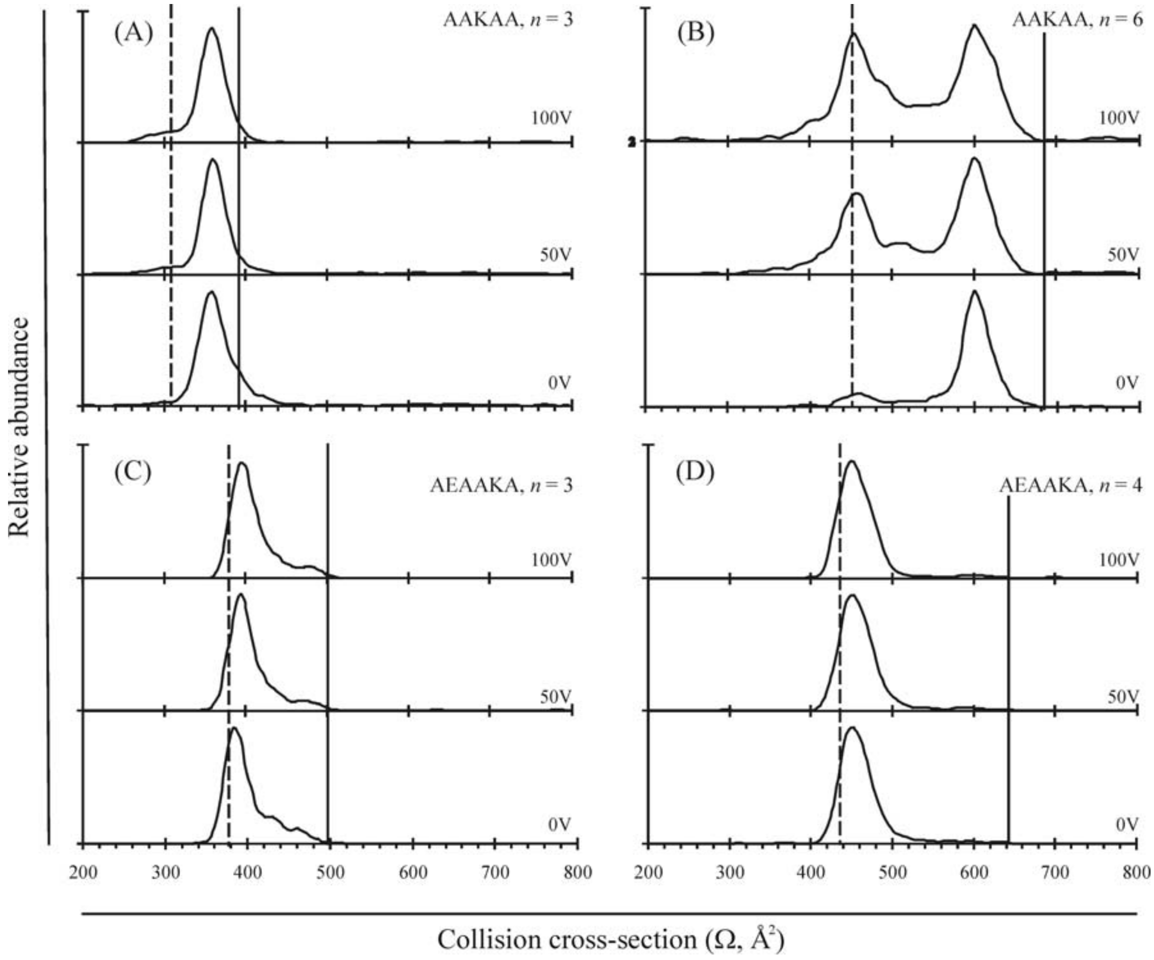

FIGURE 15. The IM profiles for $[M + H]^+$ ions of (A) Ac-$(AAKAA)_3$Y-NH_2, (B) Ac-$(AAKAA)_6$Y-NH_2, (C) Ac-Y$(AEAAKA)_3$F-NH_2 and (D) Ac-Y$(AEAAKA)_4$F-NH_2 are shown for 0, 50, and 100 V lab frame ion injection energies. The dashed vertical lines represent the predicted collision cross-sections for globular peptide mobility-mass correlation (as defined in Figure 3) and the solid vertical lines represent the α-helical mobility-mass correlation (calculated collision cross-sections for α-helices of the same amino acid sequence).

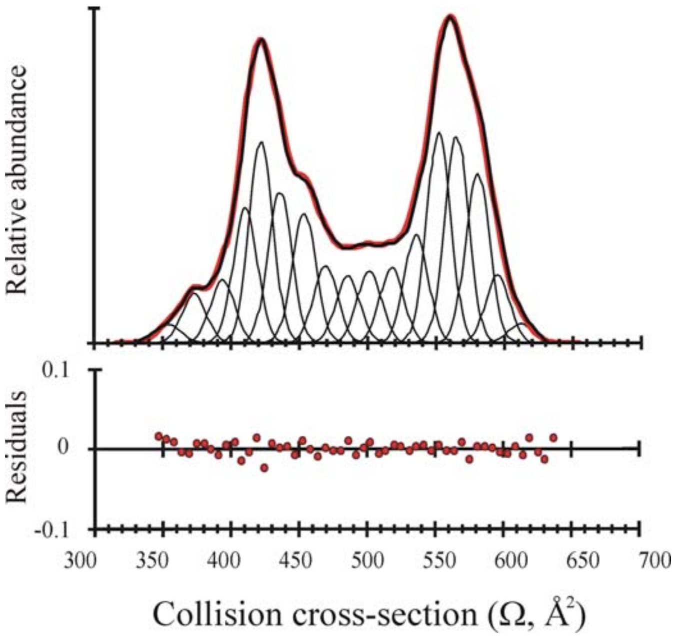

FIGURE 16. Peak deconvolution analysis constrained using peak widths derived from Monte Carlo simulations for AAKAA *n* = 6 $[M + H]^+$ ion (100 V lab frame ion injection energy, 1700 V IM separation field strength). The black line is the measured IM profile, theoretical subpopulations are shown under the measured profile and the colored lines are the composite fit. The residuals from the deconvolution analysis are shown ($R^2 > 0.99$, bottom).

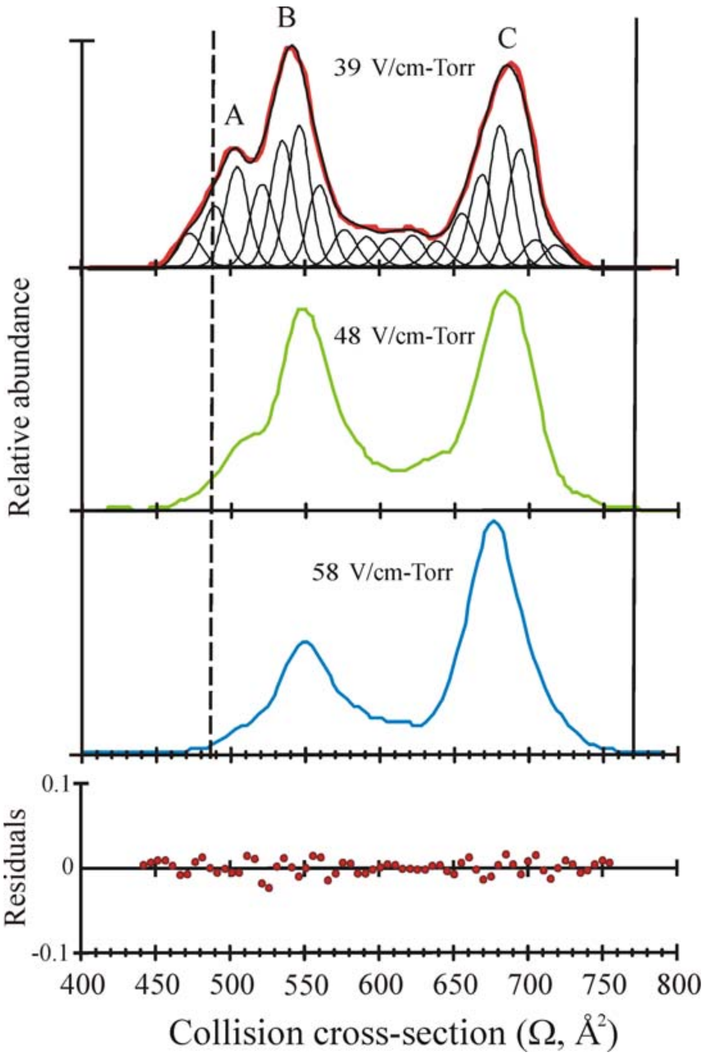

FIGURE 17. IM profiles for $[M + H]^+$ Ac-(AAKAA)$_7$Y-NH$_2$ for various field strengths (indicated in the figure) accessed by changing the pressure in the drift cell while maintaining a constant potential across the drift cell. The globular (dashed lines) and helical (solid lines) mobility-mass correlations are shown for comparison (defined in Figure 3). The letters in the top panel correspond to three structural populations (see text for details).

top panel of Figure 17 is peak deconvolution analysis for AAKAA n = 7 which illustrates the large number of structural sub-populations which remain unresolved in the peak profile. On the other hand, the AEAAKA peptides do not undergo structural change upon ion heating for any peptide length (Figure 15C and D), presumably because intramolecular charge solvation is significant enough that temperatures high enough to elicit structural change (*i.e.* break multiple non-bonding E/K or peptide-proton interactions) are not achieved in these experiments.

Results from the Jarrold laboratory for $[M + H]^+$ ions of polyalanine (polyA) are quite different (29; 35) than for the AAKAA or AEAAKA peptides in these studies. Gas-phase $[M + H]^+$ ions of polyA are not all helical, presumably because the charge is located at the N-terminus which destabilizes helical structure (29; 79). Blocking of the N-terminus by acetylation and insertion of a basic site (K) at the C-terminus results in a rigid helix for the $[M + H]^+$ ion of Ac-polyA-K (29). However, as evidenced by the structural trends reported here for acetylated AAKAA and AEAAKA peptides, a blocked N-terminus and a C-terminal basic site alone are not sufficient for stabilization of gas-phase helices. One reason helices may not be as energetically-favored in the AAKAA and AEAAKA systems is due to the location of the C-terminal K residue which is removed from the C-terminus by 2 or 3 residues, making helix capping by the charge less efficient. The location of basic sites is similar between the AAKAA and AEAAKA peptides and so it is unlikely basic site location alone accounts for the lower helical content of AEAAKA series. It is more likely that the presence of multiple basic and/or acidic residues contributes more significantly to the prevailing structural stabilities observed for the AAKAA and AEAAKA systems.

There are several possibilities to rationalize why multiple basic and acidic sites (AEAAKA) might contribute more significantly to globule stabilization (helix destabilization) than multiple basic sites alone (AAKAA). Sudha and co-workers demonstrated that insertion of an E/K pair into Ac-$A_3G_{12}K$ decreased gas-phase helical structure compared to the unsubstituted peptide ion (84). They suggested that the main reason for decreased helical content was competition for backbone H-bonds and stabilization of the globular conformation. In the AAKAA peptides, the lysine side chains may compete for helix H-bonds and destabilize helical structure, resulting in detection of partial helices. For the AEAAKA peptides, we suspect that predominantly globular structures are observed because the side chains and charge are heavily coordinated due the polar side chains (note that E is more polar than K), which stabilizes the globular conformation via charge-dipole, dipole-dipole and other interactions. Additionally, the energetic cost associated with exposing hydrophilic/polar residues to vacuum (as they would be in the helical conformation) likely outweighs the stability gained by helix formation. Note that at neutral pH in aqueous solution the E and K side chains are charged and so charge-charge interactions act to stabilize helices. However, for $[M + H]^+$ ions, only one charge site is present (K side chain) and so the E/K charge-charge interactions are not present to stabilize helical structure. Furthermore, the

AEAAKA peptides have E/K pairs which may facilitate proton transfer, and thus charge mobility may also affect helical content in the AEAAKA series.

CHAPTER IV

ANHYDROUS STRUCTURE OF ALKALI METAL-COORDINATED PEPTIDES

Introduction

Alkali metal ions play essential roles in biological systems. Specifically, Na^+ and K^+ ions are involved in enzyme activation, action potential propagation in neurons, and membrane ion transporter structure and regulation (87; 88). Specialized transport proteins are required to allow movement of ions across the low dielectric barrier of the cell membrane. Ion transport across cell membranes has been extensively studied and has revealed a role for ions in channel structure and gating (89-91).

Although structural characterization of ion channels and their interactions with metal ions is challenging due to the insolubility of membrane proteins in water, a number of groups have overcome this obstacle by adding detergents to solubilize ion channels, crystallizing the mixture, and performing X-ray crystallography experiments (91; 92). Furthermore, metal ion binding sites have been located in these ion channel structures, often near the C-terminus of α-helices, the most common secondary structure element in membrane proteins (81). Based on the location and coordination of the metal ions, it has been suggested that they stabilize helices by favorable interaction of the positive charge with the negative end of the helix macrodipole (89; 90; 92; 93). Recently, Boudker and colleagues reported Na^+ binding sites in a sodium-dependent aspartate transporter which contribute to substrate binding and channel gating (90). Thus, understanding how metal ions affect peptide and protein structure in low dielectric environments may potentially reveal the underlying interactions important for ion binding, specificity and transport.

Anhydrous studies of polyalanine-based peptides using IM-MS have shown that alkali metal ions bind near the C-terminus, thereby stabilizing helical structure by favorable interaction of the charge and the helix macrodipole (49; 50). The effect of primary sequence or number of basic/acidic sites on alkali metal ion helix stabilization has not been well-characterized.

Chapter II described IM-MS data for protonated peptides of two model peptide systems—Ac-(AAKAA)$_n$Y-NH$_2$ (n = 3, 4, 5, 6 and 7) and Ac-Y(AEAAKA)$_n$F-NH$_2$ (n = 2, 3, 4, and 5). The results indicate that gas-phase helical structure is dependent on amino acid sequence and peptide length. For the AAKAA series, the collision cross-sections for the $[M + H]^+$ species correlated with partial helices. However, for the longest peptides, n = 6 and 7 (corresponding to 31 and 36 residues, respectively), the ion IM profiles became bimodal with collision cross-sections corresponding to charge-solvated globules and partial helices. In contrast, the AEAAKA peptides exhibited very little helical content. The IM profile for the shortest $[M + H]^+$ AEAAKA (n = 2) peptide was very broad with the average collision cross-section corresponding to a partial-helix. For the longer AEAAKA $[M + H]^+$ ions, only a population corresponding to charge-solvated globules was detected. Here, we use IM-MS to probe the anhydrous structure of these model peptides to understand the effect of metal-coordination on ion structure.

Results and discussion

Alkali metal ions are important in protein structure and enzyme activity, especially in membrane transporter proteins (87). Thus, it is important to understand how metal ions affect peptide structure and stability in a low dielectric environment (*i.e.* similar to that of the cell membrane). We have used IM-MS to measure collision cross-sections for the metal-coordinated ions of Ac-(AAKAA)$_n$Y-NH$_2$ (n = 3, 4, 5, 6 and 7) and Ac-Y(AEAAKA)$_n$F-NH$_2$ (n = 2, 3, 4, and 5), hereafter simply referred to as AAKAA and AEAAKA, in an effort to understand the effect of metal ion coordination on anhydrous peptide structure. These peptide systems were originally developed in the R. L. Baldwin laboratory to study the effect of peptide length on solution-phase helical content; CD studies showed that the helical content of the AAKAA and AEAAKA peptides increases with peptide length (54; 55). See Chapter I for further information on these systems and justification for their use in these studies.

Figure 18 contains IM-MS data plotted as abundance of $[M + Na]^+$ ions versus IM drift time (t_d, upper axes) and collision cross-section (Ω, lower axes) for the AAKAA (n = 3 - 7) and AEAAKA (n = 2, 3, 4, and 5) peptide ions. A plot of the average collision cross-section of $[M + X]^+$ (where X = Li, Na, K, Rb, Cs) versus the averaged mass-to charge (m/z) for all metal-coordinated peptides (Figure 19) reveals that structural trends for the

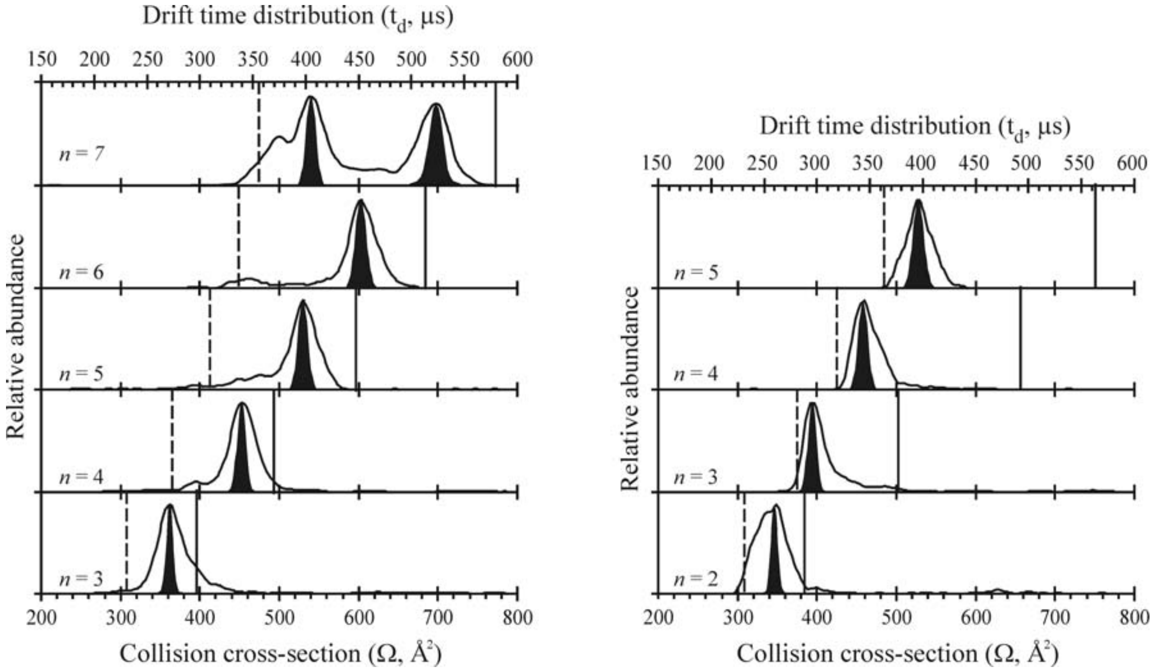

FIGURE 18. IM drift time (upper x-axis) and collision cross-section (lower x-axis) profiles for [M + Na]$^+$ of (A) Ac-(AAKAA)$_n$Y-NH$_2$ (n = 3, 4, 5, 6, and 7) and (B) Ac-Y(AEAAKA)$_n$F-NH$_2$ (n = 2, 3, 4, and 5). The dashed vertical lines represent the predicted collision cross-sections for globular peptide mobility-mass correlation (as defined in Figure 3) and the solid vertical lines represent the α-helical mobility-mass correlation (calculated collision cross-sections for α-helices of the same amino acid sequence). The shaded profiles are simulated IM profiles for a single collision cross-section, assuming peak broadening arises only from longitudinal diffusion.

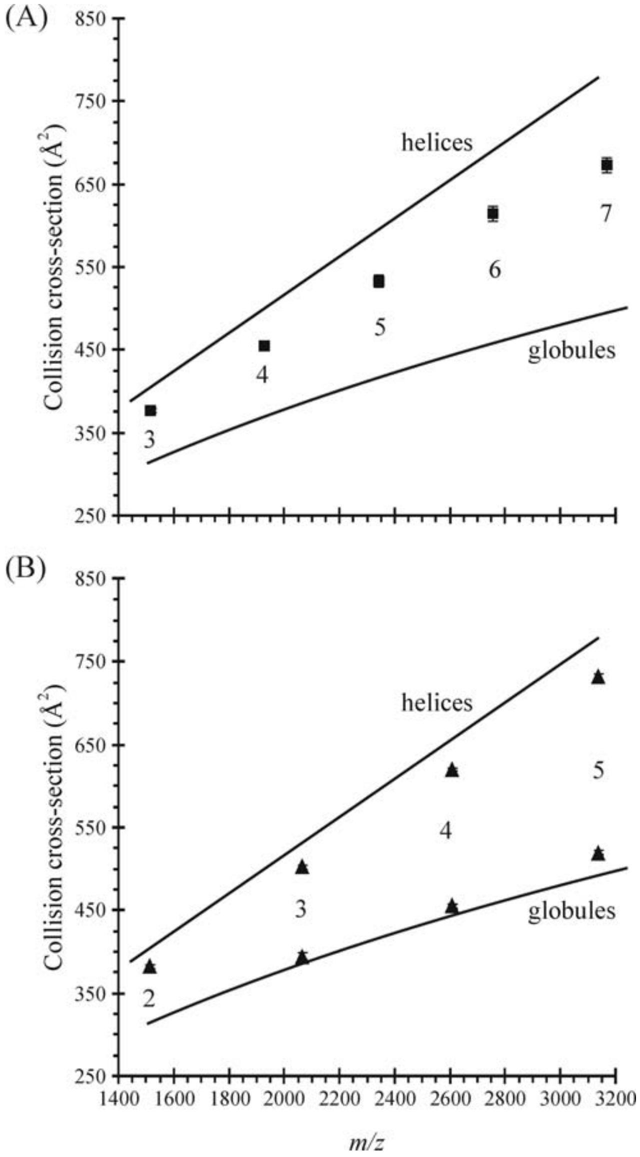

FIGURE 19. Plot of the composite alkali metal-coordinated peptide collision cross-sections versus average *m/z* for $[M + X]^+$ (X = Li, Na, K, Rb, or Cs) ions for (A) AAKAA (■) and (B) AEAAKA (▲), *i.e. e*ach point is the average of all $[M + X]^+$ collision cross-sections for that peptide. The lines represent the globular and helical mobility-mass correlations (as defined in Figures 3 and 9). The labels correspond to the number of peptide repeats (*n*). Error bars represent ±1 σ for 25 measurements.

metal-coordinated ions are dependent on primary sequence. The AAKAA metal-coordinated ions exhibit collision cross-sections which are intermediate between the expected globular and helical mobility-mass correlations, regardless of peptide length (Figure 19A). However, the anhydrous structure of the metal-coordinated AEAAKA ions is peptide length dependent. Metal-coordinated species of the shortest peptide (n = 2) exhibit a collision cross-section indicative of a helix. However, as peptide repeats are added, the metal-coordinated species exhibit bimodal distributions, as indicated in Figure 19B for n = 3, 4, and 5.

The absolute difference in collision cross-section between globular and helical structures increases as peptide length increases because helix propagation impacts the collision cross-section more per amino acid due to the aspect ratio of a helix (approximated by a cylinder) compared to a globule (approximated by a sphere) (85). Thus, conversion of the measured collision cross-sections to helical content (Eq. 6) normalizes the dataset for both relative abundance of the extended population and the mass-dependent relative difference between globular and helical collision cross-sections, allowing us to examine structural trends as a function of peptide length. Comparison of the helical content of $[M + X]^+$ for the AAKAA peptides to the AEAAKA peptides (Figure 20) reveals that the AAKAA peptides exhibit similar helical content regardless of length (or number of polar residues), whereas helical content consistently decreases with peptide length and addition of polar residues in the AEAAKA series. Although these same general trends in helical content were observed for the $[M + H]^+$ of these series (94), alkali metal

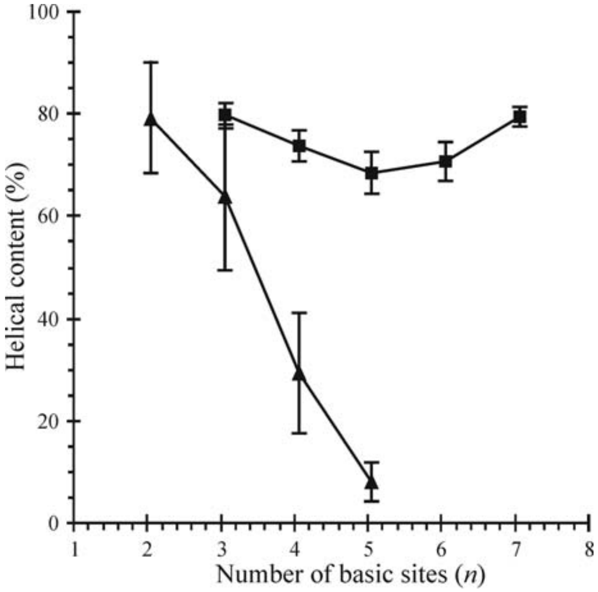

FIGURE 20. Plot of average helical content (Eq. 6) for all metal-coordinated species $[M + X]^+$ (X = Li, Na, K, Rb, or Cs) ions (each point is the average of all $[M + X]^+$ collision cross-sections for that peptide) versus number of basic amino acid residues for the AAKAA (■) and AEAAKA (▲) peptides. Error bars represent ±1 σ for 25 measurements.

coordination results in overall higher helical content for both peptide series, suggesting that alkali metals stabilize *some* helical structure regardless of the amino acid sequence investigated here. The decrease in overall helical content with increasing peptide length in the AEAAKA (and *not* AAKAA) suggests that it is the *combination* of E/K residues which destabilizes helices or stabilizes globules. This trend could be due to competition of E/K side chains for backbone H-bonds (as has been suggested previously (84)) or a shift in the energetic balance between globule and helix caused by participation of the E/K side chains in metal ion coordination, *i.e.* formation of charge-solvated ion structures.

The effect of specific alkali metals on helical content is shown in Figure 21. For the AAKAA series, helical content remains relatively constant for all species (60 – 80 %). Interestingly, the collision cross-sections for $[M + Li]^+$ are intermediate between $[M + H]^+$ and the other alkali metals (see Table 2, for all collision cross-sections); this could be a consequence of the high charge density of Li^+ compared to the other alkali metals (95) which may be better solvated in globular conformations. The metal-coordinated ions of the AEAAKA series exhibit collision cross-sections which depend on ion type and peptide length (Figure 21B, Table 3). Helical content decreases with increasing peptide length, regardless of ion type, but the range of helical content for each peptide length is large, as evidenced by the large error bars in Figure 20. In the AEAAKA series, helical content increases with increasing ionic radius (Cs > Rb > Na > Li) for all

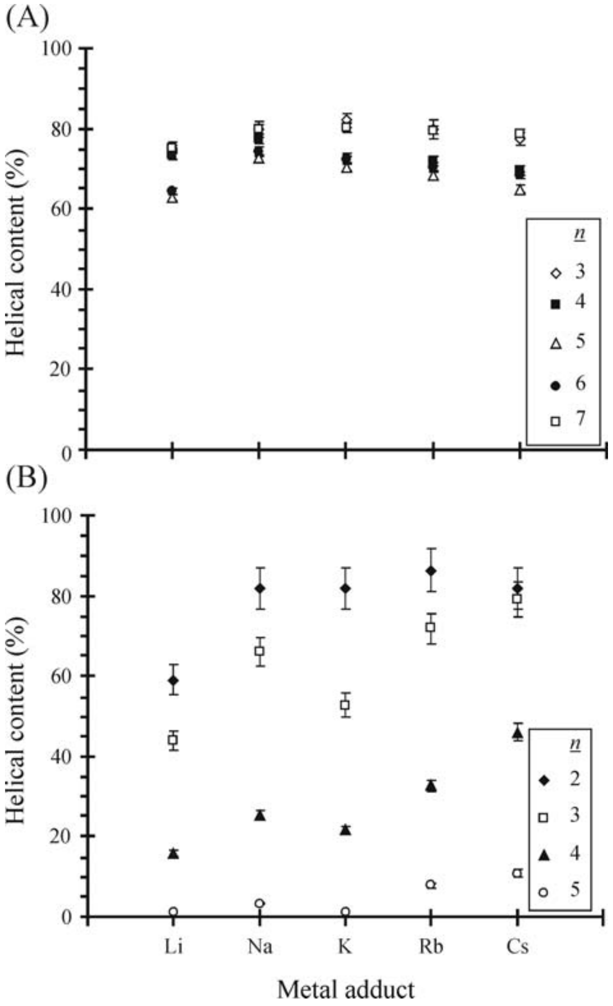

FIGURE 21. Plot of helical content (Eq. 6) versus metal-coordinated $[M + X]^+$ (X = Li, Na, K, Rb, or Cs) species for (A) AAKAA and (B) AEAAKA. In the legends, *n* is the number of peptide repeats. Error bars represent ±1 σ for 5 measurements.

TABLE 2. Mass-to-charge ratios (*m/z*), collision cross sections (Ω) and reduced mobilities (K_o) for $[M + X]^+$ ions for Ac-(AAKAA)$_n$Y-NH$_2$ (*n* = 3, 4, 5, 6 and 7) where *n* = the number of peptide repeats. Mass-to-charge values are reported as average mass. Collision cross-sections and reduced mobilities are reported with error corresponding to ± 1 σ for m measurements.

	n	species	*m/z*	Ω (Å^2)	K_o	M
Ac-(AAKAA)$_n$Y-NH$_2$	3	$[M+Li]^+$	1466.65	374 ± 2	1.441 ± 0.007	10
		$[M+Na]^+$	1482.72	378 ± 5	1.423 ± 0.019	10
		$[M+K]^+$	1498.80	372 ± 3	1.323 ± 0.007	10
		$[M+Rb]^+$	1545.18	378 ± 8	1.329 ± 0.025	10
		$[M+Cs]^+$	1592.62	376 ± 2	1.335 ± 0.008	10
	4	$[M+Li]^+$	1879.14	455 ± 4	1.184 ± 0.010	10
		$[M+Na]^+$	1895.21	460 ± 4	1.169 ± 0.011	10
		$[M+K]^+$	1911.29	454 ± 5	1.185 ± 0.012	10
		$[M+Rb]^+$	1957.67	453 ± 3	1.196 ± 0.009	10
		$[M+Cs]^+$	2005.11	450 ± 2	1.113 ± 0.007	10
	5	$[M+Li]^+$	2291.63	524 ± 2	1.028 ± 0.004	10
		$[M+Na]^+$	2307.68	542 ± 4	0.994 ± 0.009	10
		$[M+K]^+$	2323.78	538 ± 2	1.000 ± 0.004	10
		$[M+Rb]^+$	2370.16	534 ± 2	1.007 ± 0.004	10
		$[M+Cs]^+$	2417.60	528 ± 3	1.019 ± 0.006	10
	6	$[M+Li]^+$	2704.12	601 ± 2	0.895 ± 0.004	10
		$[M+Na]^+$	2720.19	624 ± 6	0.862 ± 0.009	10
		$[M+K]^+$	2736.30	619 ± 2	0.868 ± 0.003	10
		$[M+Rb]^+$	2782.67	615 ± 2	0.874 ± 0.003	10
		$[M+Cs]^+$	2830.11	610 ± 3	0.881 ± 0.004	10
	7	$[M+Li]^+$	3116.61	656 ± 3	0.820 ± 0.004	9
		$[M+Na]^+$	3132.66	678 ± 8	0.98 ± 0.098	10
		$[M+K]^+$	3148.77	679 ± 8	0.798 ± 0.001	9
		$[M+Rb]^+$	3195.14	679 ± 7	0.800 ± 0.002	9
		$[M+Cs]^+$	3242.58	676 ±7	0.803 ± 0.002	9

TABLE 3. Mass-to-charge ratios (*m/z*), collision cross sections (Ω) and reduced mobilities (K_o) for $[M + X]^+$ ions for Ac-Y(AEAAKA)$_n$F-NH$_2$ (n = 2, 3, 4, and 5) where n = the number of peptide repeats and subscripts indicate compact (c) or extended (e) conformations. Mass-to-charge values are reported as average mass. Collision cross-sections and reduced mobilities are reported with error corresponding to ± 1 σ for m measurements.

	n	species	*m/z*	Ω (Å^2)	K_o	m
Ac-Y(AEAAKA)$_n$F-NH$_2$	2	$[M+Li]^+$	1459.57	378 ± 5	1.421 ± 0.020	3
		$[M+Na]^+$	1475.62	383 ± 3	1.405 ± 0.010	10
		$[M+K]^+$	1491.73	383 ± 4	1.403 ± 0.013	5
		$[M+Rb]^+$	1538.10	385 ± 2	1.399 ± 0.006	4
		$[M+Cs]^+$	1585.54	383 ± 2	1.405 ± 0.008	4
	3	$[M+Li]^+_c$	2001.18	390 ± 4	1.379 ± 0.013	3
		$[M+Li]^+_e$	2001.18	498 ± 8	1.081 ± 0.017	3
		$[M+Na]^+_c$	2017.23	393 ± 6	1.369 ± 0.022	10
		$[M+Na]^+_e$	2017.23	503 ± 3	1.071 ± 0.006	10
		$[M+K]^+_c$	2033.34	395 ± 1	1.364 ± 0.003	8
		$[M+K]^+_e$	2033.34	503 ± 4	1.069 ± 0.008	9
		$[M+Rb]^+_c$	2079.71	397 ± 4	1.354 ± 0.014	4
		$[M+Rb]^+_e$	2079.71	505 ± 3	1.065 ± 0.006	4
		$[M+Cs]^+_c$	2127.14	400 ± 5	1.346 ± 0.016	3
		$[M+Cs]^+_e$	2127.14	503 ± 3	1.069 ± 0.006	4
	4	$[M+Li]^+_c$	2542.78	452 ± 6	1.190 ± 0.016	3
		$[M+Li]^+_e$	2542.78	619 ± 12	0.870 ± 0.017	3
		$[M+Na]^+_c$	2558.83	456 ± 4	1.180 ± 0.011	10
		$[M+Na]^+_e$	2558.83	620 ± 5	0.868 ± 0.008	9
		$[M+K]^+_c$	2574.94	455 ± 4	1.183 ± 0.007	10
		$[M+K]^+_e$	2574.94	618 ± 8	0.871 ± 0.011	6
		$[M+Rb]^+_c$	2621.31	456 ± 2	1.181 ± 0.006	4
		$[M+Rb]^+_e$	2621.31	621 ± 7	0.866 ± 0.010	4
		$[M+Cs]^+_c$	2668.75	457 ± 3	1.178 ± 0.007	4
		$[M+Cs]^+_e$	2668.75	622 ± 4	0.865 ± 0.006	4
	5	$[M+Li]^+_c$	3084.39	519 ± 7	1.045 ± 0.013	3
		$[M+Na]^+_c$	3100.44	517 ± 5	1.041 ± 0.009	10
		$[M+Na]^+_e$	3100.44	727 ± 11	0.74 ± 0.012	8
		$[M+K]^+_c$	3116.53	518 ± 6	1.043 ± 0.012	9
		$[M+Rb]^+_c$	3162.91	523 ± 2	1.028 ± 0.004	4
		$[M+Rb]^+_e$	3162.91	735 ± 4	0.732 ± 0.004	4
		$[M+Cs]^+_c$	3210.35	520 ± 2	1.035 ± 0.003	4
		$[M+Cs]^+_e$	3210.35	732 ± 3	0.735 ± 0.003	4

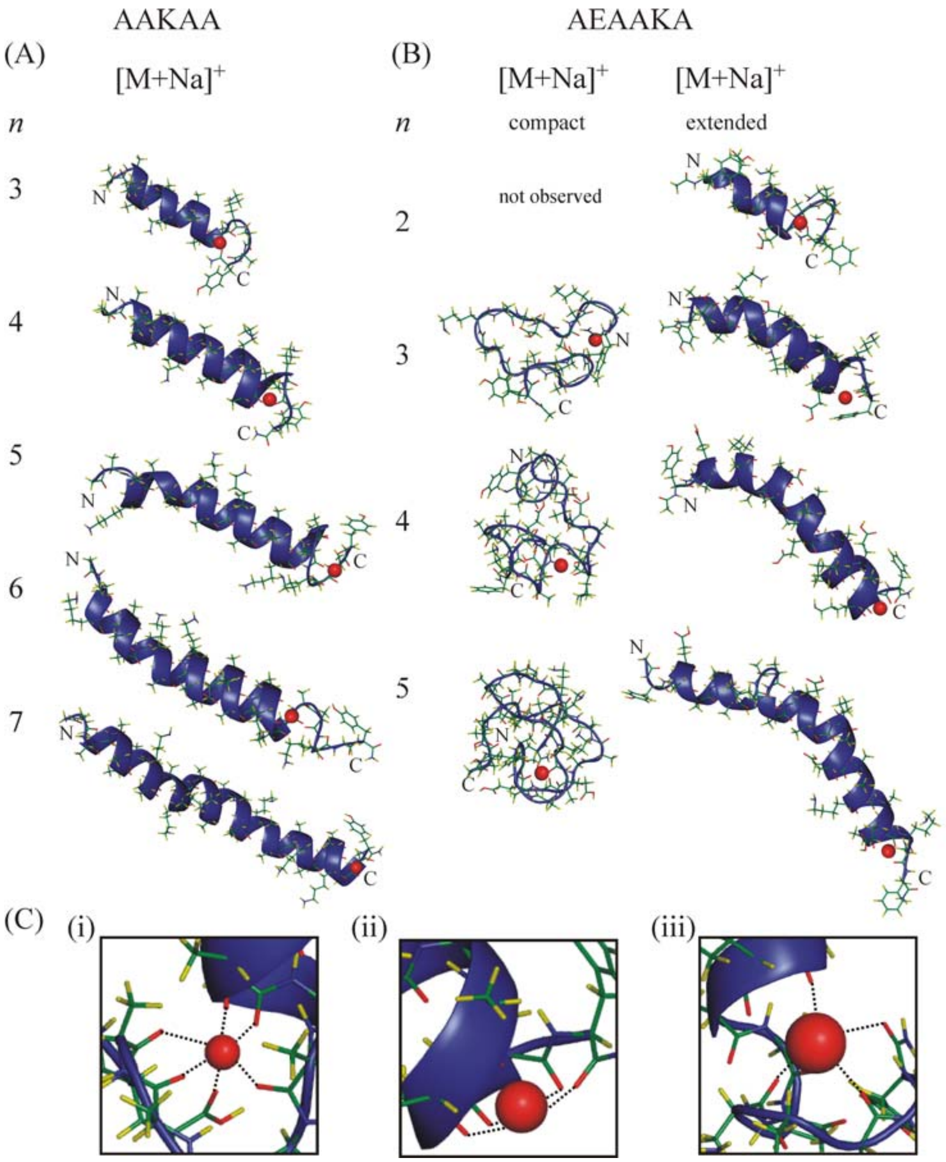

FIGURE 22. The lowest energy structures generated using molecular dynamics for [M + Na]$^+$ ions for (A) Ac-(AAKAA)$_n$Y-NH$_2$ (n = 3, 4, 5, 6 and 7) and (B) Ac-Y(AEAAKA)$_n$F-NH$_2$ (n = 2, 3, 4, and 5). (C) Magnified images of ion-peptide interactions in model structures. (i) Li$^+$ coordination by backbone carbonyl oxygens in Ac-Y(AEAAKA)$_3$F-NH$_2$ (ii) Na$^+$ coordination by backbone carbonyl oxygen atoms of Ac-Y(AEAAKA)$_4$F-NH$_2$, and (iii) K$^+$ coordination by backbone carbonyl structure oxygen atoms of Ac-(AAKAA)$_3$Y-NH$_2$. Na$^+$, Li$^+$ and K$^+$ are depicted as red spheres. Coordination to the metal by oxygen atoms is denoted with dashed black lines. “N” and “C” indicate the N- and C- termini, respectively.

peptide lengths, with the exception of $[M + K]^+$, which exhibit lower helical content than $[M + Na]^+$ or $[M + Rb]^+$ ions.

Molecular models were generated for all species. Models for the other alkali metals were similar to the results for $[M + Na]^+$, so for simplicity, we will discuss model structure mainly in terms of the Na^+-coordinated species. Models which correlate with the measured collision cross-sections for the $[M + Na]^+$ AAKAA ions (Figure 22A) are all distorted helices. The AAKAA metal-coordinated collision cross-sections are significantly larger than predicted by the globular mobility-mass correlation (see Figure 19A), but somewhat smaller than rigid α-helices. This pattern could potentially indicate π-helices (smaller collision cross-sections than α-helices), but calculation of π-helical collision cross-sections for these sequences only reveals a 3% difference between the two helix types, a difference that is too small to resolve with our current instrumentation. Therefore, we can not rule out the possibility that these ions are indeed π-helices or a mixture of α- and π- helices, but the models generated by simulated annealing (Figure 22A) indicate bent or distorted extended α-helices for all $[M + Na]^+$ AAKAA ions, which are structural elements common in proteins which specifically bind Na^+ ions (87). Also, Kohtani and co-workers reported distortion of the C-terminus of helices in metal-coordinated ions, suggesting that metal coordination often results in distortion of the helical backbone (49).

The structural trends for AEAAKA $[M + Na]^+$ are different and depend on peptide length. Molecular models for the shortest peptide (n = 2) indicate helical conformations for $[M + Na]^+$ ions. The bimodal distributions for n = 3, 4, and 5 are composed of two populations—compact and extended. The model structures for the compact conformers of n = 3, 4, and 5 are charge-solvated globules (Figure 22B), as expected from the correlation between the predicted globular collision cross-section and the experimentally-determined values (Figure 19B). The collision cross-sections of the extended conformations of n = 3, 4, and 5 approximate the α-helical mobility-mass correlation and the lowest energy molecular models are indeed α-helices (Figure 22B). Several IM profiles for the AEAAKA ions extend slightly beyond the ideal α-helical mobility-mass correlation (see for example Figure 18, AEAAKA n = 3) which could indicate the presence of 3/10 helical segments because the collision cross-sections of 3/10-helices are significantly larger (*ca*. 7-15%) than α- or π- helices (Figure 23). However, the lowest energy models for the extended populations of the AEAAKA ions do not contain 3/10 helical components and thus we assign the extended AEAAKA ions to α-helices.

The average percent helix (α, π and 3_{10} combined) in the 10 lowest energy structures for each peptide generated by molecular modeling is consistent with the experimental results (Figure 24). For instance, the percent helix of the model structures is highest for the extended conformers of the $[M + Na]^+$ AEAAKA species (54%), lowest in the compact conformers of the AEAAKA series (10%), and intermediate in ions of the AAKAA

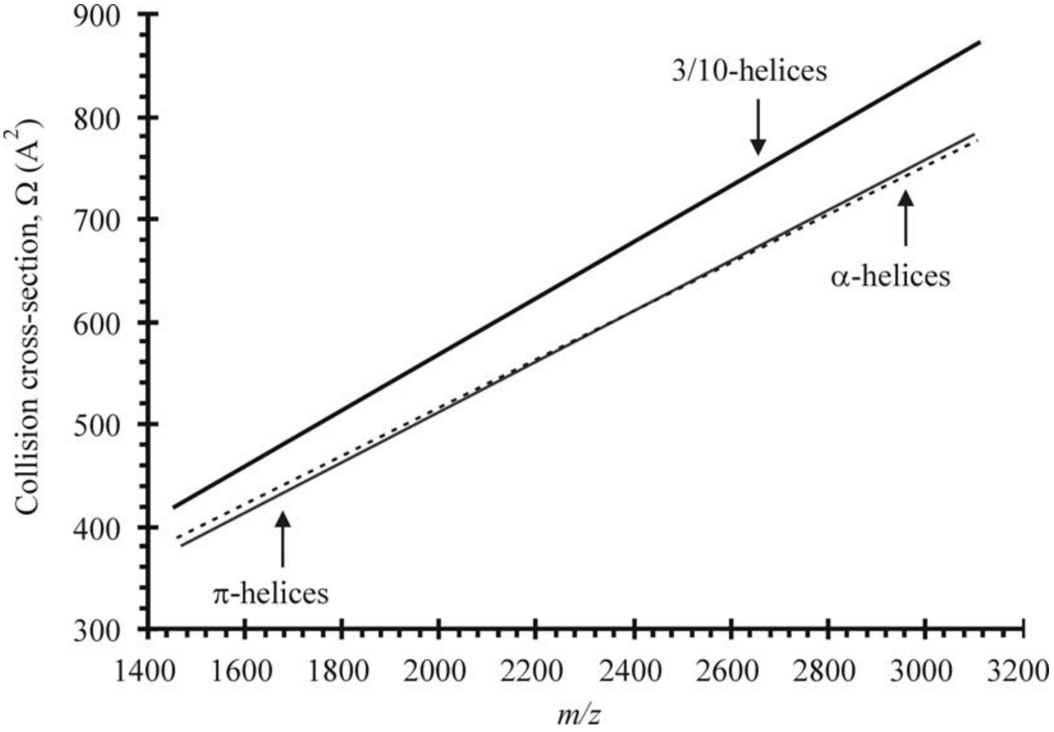

FIGURE 23. Mobility-mass correlations for the three types of helices for AAKAA and AEAAKA peptide $[M + H]^+$ ions (for details see Chapter II, *Molecular modeling*).

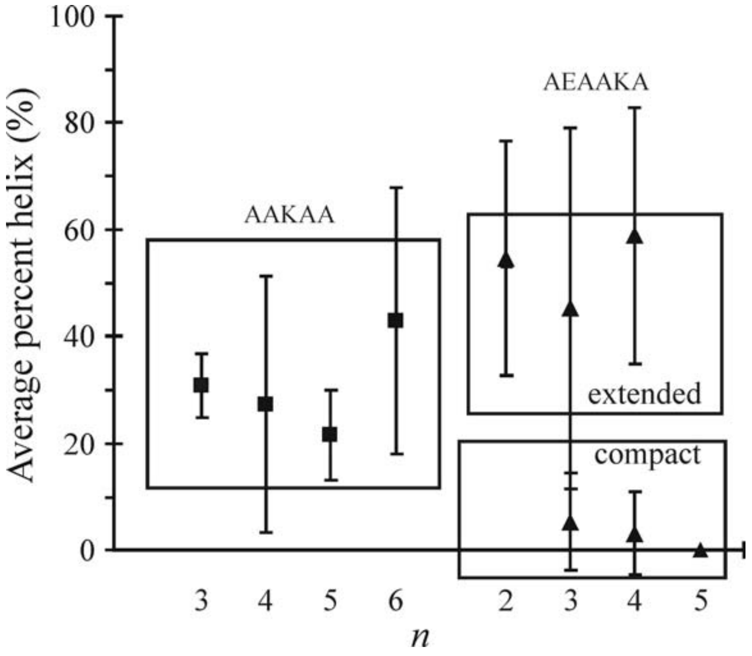

FIGURE 24. Average percent helix of the 10 lowest energy model structures which match the measured collision cross-sections for $[M + Na]^+$ for Ac-$(AAKAA)_n$Y-NH_2 (n = 3, 4, 5, and 6, ■) and Ac-Y$(AEAAKA)_n$F-NH_2 (n = 2, 3, 4, and 5, ▲). The average percent helix was calculated using the Kabsch Sander definitions (34; 75). Error bars represent ±1 σ for 10 structures.

series (34%). This trend agrees with the experimental helical content data (Figure 21), although the absolute values are lower in the modeled structures; this may be a consequence of the strict parameterization of the model used to define the secondary structural elements (*i.e.* only residues with i, i+3; i, i+4, or i, i+5 H-bonds are considered helical) (75).

We have critically evaluated our structural assignments for the AEAAKA ions by examining the torsion angle space of the $[M + Na]^+$ ions for $n = 4$. The range of allowed backbone torsion angles (dihedral angles), denoted Φ ($N \rightarrow C_\alpha$ bond angle) and Ψ ($C_\alpha \rightarrow C_{c=o}$ bond angle), are determined by the physicochemical characteristics of the peptide (Figure 25). For example, only certain angle pairs are energetically-favored for specific amino acids depending on bond and steric constraints (96). Various Φ and Ψ pairs are indicative of secondary structure elements such as α-helices ($\Phi = -57°$, $\Psi = -47°$) or β-sheets ($\Phi = -60$ to -180, $\Psi = 60$ to 180). Thus, the Ramachandran plot can be used to assess peptide and protein secondary structure by visualizing the individual Φ and Ψ pairs for each amino acid in a peptide sequence. The torsion angles of the extended conformations of the AEAAKA series are consistent with α-helices (Figure 26, region A) but the globular conformations populate torsion angle space corresponding to non-specific, “random” secondary structure (Figure 26, region C). The AEAAKA globules sample several disallowed (energetically-unfavorable) torsion angle regions, which are indicative of unfolded proteins in solution (97; 98), *i.e.* the dominant

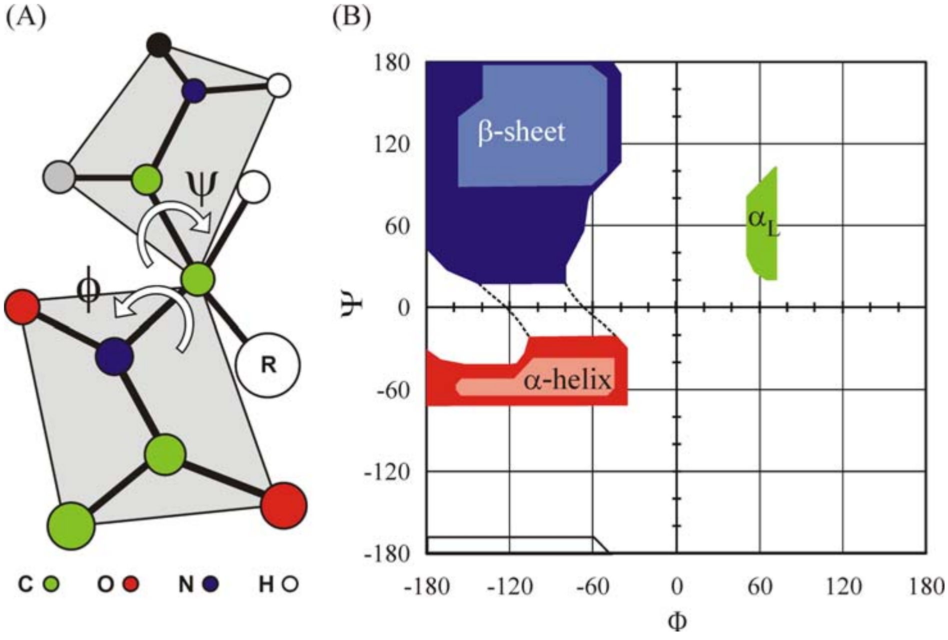

FIGURE 25. Peptide torsion angles**.** (A) Illustration of peptide torsion angles Φ (N→C$_\alpha$ bond angle) and Ψ (C$_\alpha$→C$_{c=o}$ bond angle). (B) Allowed Φ and Ψ torsion angle space for alanine (Adapted from Ref. 96).

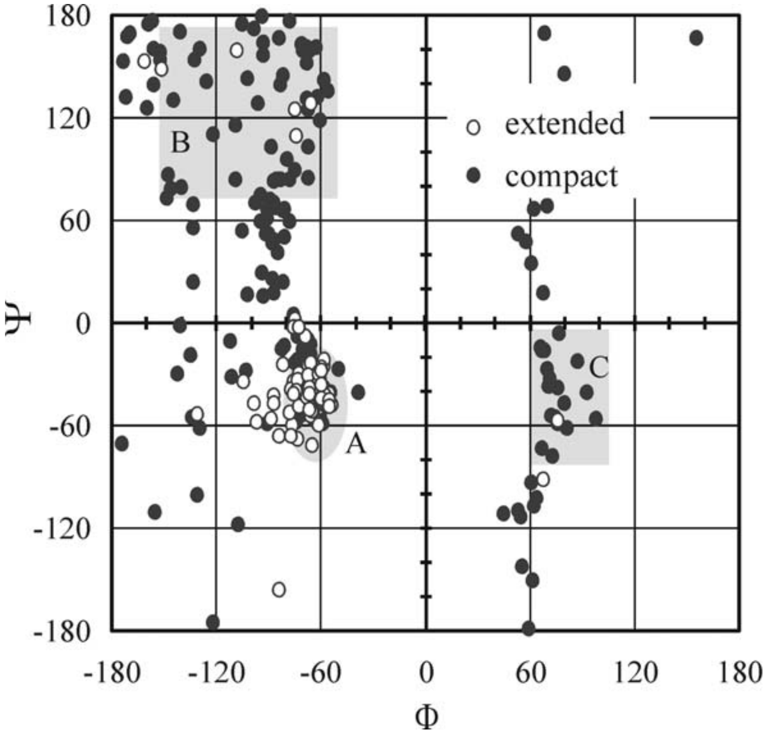

FIGURE 26. Ramachandran plot for simulated AEAAKA peptide (*n* = 4) structures which match the empirical collision cross-sections for globular (compact) and helical (extended) conformations. (A) denotes region indicative of α-helices, (B) denotes region indicative of β-structure and (C) denotes a representative disallowed region. Each data point represents a Φ and Ψ torsion angle pair for one amino acid as defined in Figure 25.

intramolecular interactions in charge-solvated ions are not ordered and result in “random” structures.

In general, the IM peak widths for globular conformations are broader than those attributed to helical conformations (Figure 27A). Owing to this relationship between peak width and ion conformation, we performed extensive analysis of the peak profiles for the $[M + Na]^+$ AEAAKA $n = 4$ ion using ion trajectory simulations developed by Raznikov and co-workers (68). From these calculations, we can estimate the expected peak profiles (shaded region of Figure 27A) for a population of ions corresponding to a single collision cross-section, *i.e.* an ensemble of closely-related structures, assuming peak broadening arises exclusively from ion diffusion. The peak width of the helical component corresponds well with the simulated peak (residuals are shown in the bottom panel). We also applied peak deconvolution analysis to estimate the number of possible conformers comprising the peak profiles. A best-fit of the helical profile corresponds to a single component peak with one minor component (labeled v and vi, respectively, middle panel, Figure 27A). The absence of multiple conformations under the helical IM profile suggests that the ion population is likely composed of a single dominant species, a rigid helix, which has few related conformations that are energetically-accessible. On the other hand, the peak profile labeled “globule” is much broader than the computed peak profile, and deconvolution analysis reveals that this peak is composed of multiple structural populations (6 - 7 components), suggesting that at least several stable, unresolved conformations are present under these experimental conditions. The

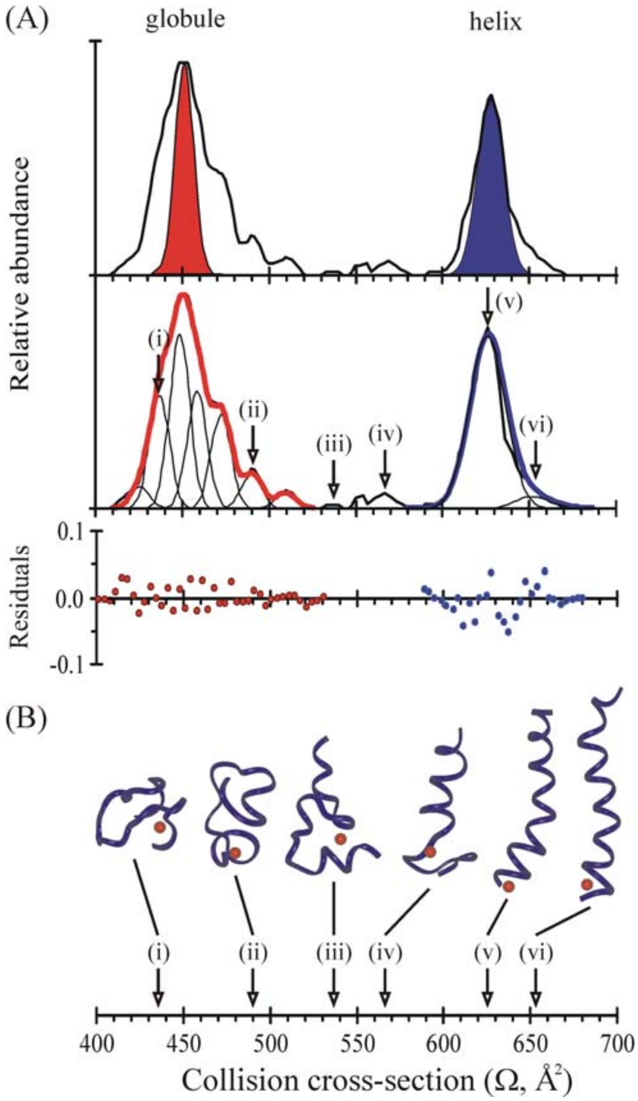

FIGURE 27. IM profile for $[M + Na]^+$ AEAAKA *n* = 4. (A) Comparison of simulated (shaded) and empirical IM profiles for $[M + Na]^+$ Ac-Y(AEAAKA)$_4$F-NH$_2$ (top). Peak deconvolution analysis constrained using peak widths derived from Monte Carlo simulations (68)(middle). The black lines are the measured IM profile and the theoretical subpopulations under the parent profile. The colored lines are the composite fit. The residuals from the deconvolution analysis are shown (red for globule and blue for helix, $R^2 > 0.99$, bottom). (B) Representative ribbon models for structures (in terms of Ω values) ranging from globular to helical conformations. The numbered peaks in part (A) correspond to the collision cross-sections of the structural models shown in part (B).

presence of multiple populations in the globular profile and only a single dominant population for the helical component may be compared to solution-phase protein folding where there are many randomly unfolded states (globular conformers), but only one or a few native states (helix).

We used ion injection techniques similar to those reported elsewhere (69) to investigate the stability of the $[M + Na]^+$ ion structural populations. This methodology consists of accelerating the ion population, so that the ions experience *ca*. 10-100 low energy collisions and are then cooled by collisions with the buffer gas and injected into the IM drift cell for structural analysis. If the ions comprising a particular population are easily converted to another structure (*i.e.* globule → helix), then we expect to observe changes in the relative peak area as a function of the ion injection voltage. Neither the AAKAA nor the AEAAKA peptides undergo significant structural changes upon ion heating for any peptide length (Figure 28), presumably because the metal is solvated by the peptide (Figure 22C(ii)) and we do not access temperatures high enough to elicit structural change, *i.e.* break multiple non-bonding E/K or ion-dipole interactions.

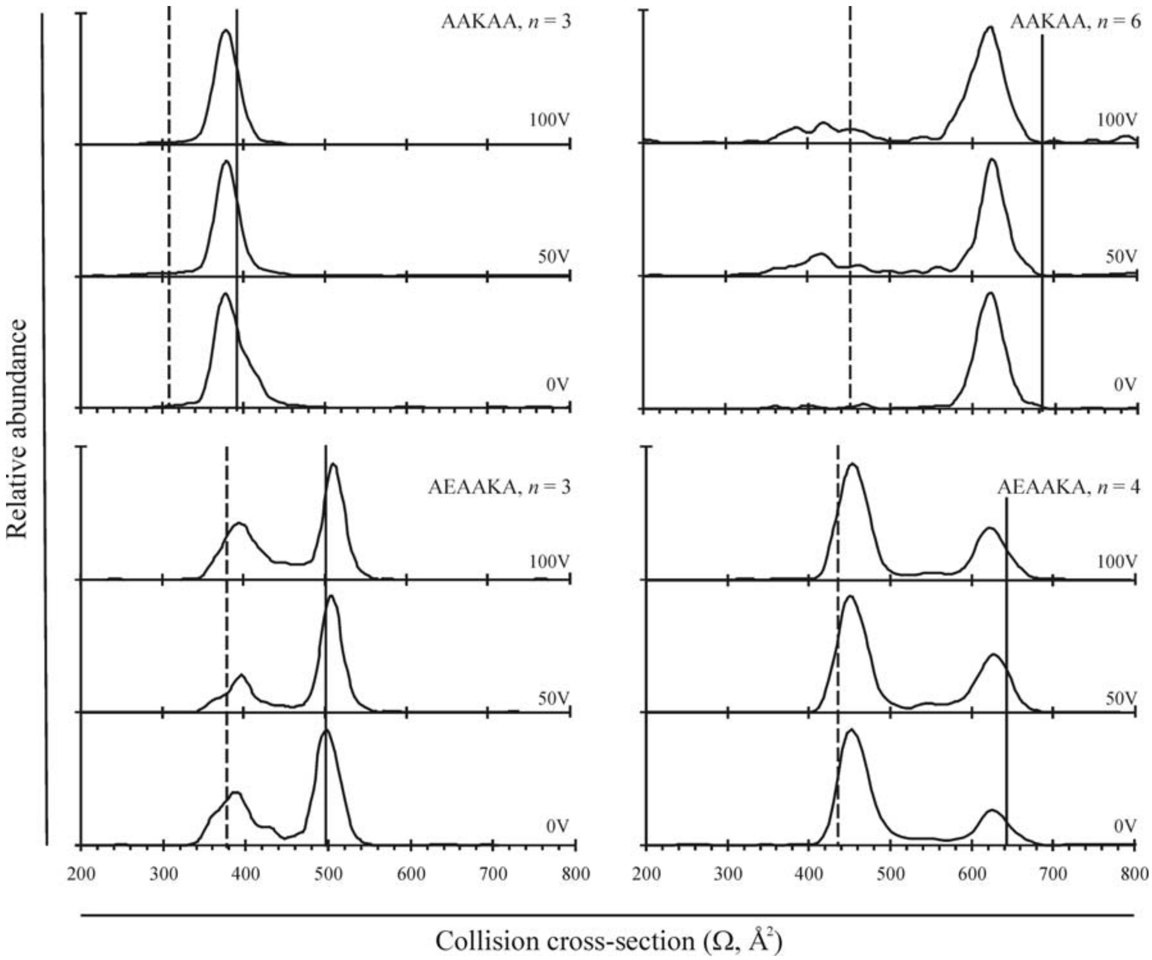

FIGURE 28. The collision cross section profiles for $[M + Na]^+$ ions of Ac-$(AAKAA)_3$Y-NH_2, Ac-$(AAKAA)_6$Y-NH_2, Ac-Y$(AEAAKA)_3$F-NH_2 and Ac-Y$(AEAAKA)_4$F-NH_2 are shown for 0, 50, and 100 V lab frame ion injection energies. The dashed vertical lines represent the predicted collision cross-sections for globular peptide mobility-mass correlation (as defined in Figure 3) and the solid vertical lines represent the α-helical mobility-mass correlation (calculated collision cross-sections for α-helices of the same amino acid sequence).

CHAPTER V

CONCLUSIONS AND FUTURE DIRECTIONS

Our results for AAKAA and AEAAKA confirm previous results (29; 30; 35) showing that the dominant gas-phase structures of alanine-containing peptides are charge-solvated globules and helices. Analysis of IM-MS and molecular modeling data for $[M + H]^+$ ions of AAKAA and AEAAKA peptides reveals that peptide structure in the gas phase is dependent on primary sequence and peptide length (Chapter III). The presence of multiple basic sites in the AAKAA series does not affect the formation of partial helices for shorter peptides (n = 3 - 5), but as peptide length increases further, globular populations become more apparent. Insertion of glutamic acid residues (AEAAKA series) results in different gas-phase structural trends where helical structure decreases as peptide length increases, much more dramatically than in the AAKAA peptides. Even though a basic site is present near the C-terminus, only the shortest (n = 2) AEAAKA peptide exhibits any gas-phase helical content. We probed the stability of the structural populations by collisional heating the ions and demonstrated that long AAKAA $[M + H]^+$ ions exhibit pronounced structural transitions, whereas AEAAKA $[M + H]^+$ ions exhibit little structural change. We attribute the increased stability of the AEAAKA ion structures to increased charge solvation by polar side chains and H-bonding as well as the energetic cost associated with exposing polar side chains to vacuum (as in the helical conformation).

Alkali metal coordination results in very different structural trends in the AAKAA and AEAAKA peptide series (Chapter IV). Helical content is related to peptide sequence, peptide length, and ion type. Li^+ is the least helix stabilizing of all the alkali metals for both peptide series. For the AAKAA peptides, distorted helices are stabilized by all the alkali metals (although to a lesser extent by Li^+) for all peptide lengths. Alkali metal coordination by the AEAAKA peptides results in helix stabilization for all peptide lengths, but the relative abundance of the helical component decreases as peptide length increases. Neither series exhibits structural transitions upon collisional heating when sodium coordinated, indicating that metal-coordinated ion structures are more stable than protonated ion structures. Together, these data show that alkali metal helix stabilization can be counterbalanced by other forces such as intramolecular interactions and charge solvation.

The results presented in Chapters III and IV demonstrate the strength of IM-MS an analytical tool to investigate the intrinsic properties of polypeptide ions with multiple basic residues and to elucidate the dominant forces that dictate structure in low dielectric environments. Although the relevance of gas-phase data to biological systems is still an open issue, it is interesting to note that gas-phase, low dielectric environments more closely approximate the estimated dielectric of the protein interior ($\varepsilon = 2 - 20$) (99; 100) or cell membrane ($\varepsilon = 2$) than aqueous solution ($\varepsilon = 80$) (37), suggesting that, in some cases, gas-phase studies may provide more accurate information than solution-based methodologies.

There are a number of exciting experiments that can grow from our knowledge of the $[M + H]^+$ and $[M + X]^+$ AAKAA and AEAAKA ions. Given the diversity of structural subpopulations represented by many of the IM profiles (see for example Chapter IV), other gas-phase structural probes, such as H/D exchange (53; 101), may shed more light on the structural populations detected by IM-MS. The IM-MS instrumental setup (Figure 4) makes H/D exchange relatively simple because a small partial pressure of D_2O can be added to the IM bath gas to perform such experiments.

The effect of MALDI sample preparation on the gas-phase structure of the AAKAA and AEAAKA systems is also an open issue. Preliminary results (data not shown) reveal no affect of solution pH or solution temperature on the ion structures sampled (maintaining all other sample preparation as outline in Chapter II). However, changing the MALDI solvent affects crystal morphology and signal intensity (102; 103), so comparison of MALDI-IM-MS results from different solvents must be addressed critically and carefully. The organic matrix used for MALDI may also impact gas-phase ion structure. Different matrices impart varying degrees of internal energy to the ions (104; 105). The internal energy of the ion may be translated into conformational rearrangement (*e.g.* from a globule to a helix). Experiments with various MALDI matrices ranging from "hot" (high internal energy ions) to "cold" (low internal energy ions) could provide information on how MALDI matrix affects gas-phase structure, allowing for more detailed interpretation of MALDI- IM-MS results.

MALDI was used as the ionization source of choice in these studies because MALDI results almost exclusively in singly-charged ions, which greatly simplifies IM-MS spectral interpretation. In addition, MALDI is more compatible with IM-MS than ESI, because it is a pulsed ion source (*i.e.* it produces ion packets which are amenable to injection into the IM drift cell). However, other groups have successfully developed IM-MS instruments using continuous ion sources (*e.g.* ESI) (106-108). Development of an ESI source on the same IM-MS instrumental platform would provide a unique opportunity to compare ion structures generated from the two ionization techniques. Thus far, the studies of AAKAA and AEAAKA have been limited to singly-charged ions, but ESI produces ions with multiple charges. This would be especially interesting in the AAKAA and AEAAKA peptides because the basic sites are dispersed along the backbone. Charge-macrodipole effects may destabilize helical segments C-terminal to the charge and result in multiple conformations (*e.g.* globule, partial helix, helix, etc.) for both AEAAKA and AAKAA peptide series.

In solution, negatively-charged residues (D, E) are found at a higher frequency near the N-terminus (39), presumably to stabilize the helix via favorable charge-dipole interactions. The studies presented in Chapters III and IV focused on the structure of positively-charged ions; however, preliminary results for the AEAAKA series (data not shown) indicate that gas-phase helices can be stabilized by location of a negative charge at the N-terminus. Location of a negative charge at the positive end of the helix macrodipole results in favorable charge-dipole interactions and helix stabilization. Gas-phase results for negative ions will provide insight into the dominant determinants of anhydrous helical structure.

A particularly intriguing avenue for biophysical studies involves the unique kinetic and thermodynamic information that can be obtained by VT-IM-MS. In the IM drift cell, water molecules can be added one by one to gas-phase peptide ions, allowing the study of partially-hydrated peptide and protein structures (109-111). Hydration experiments of the AAKAA and AEAAKA ions could potentially reveal how many water molecules are required so that the hydrated ion mimics structures determined in solution. By using VT-IM-MS, the equilibrium constant for the hydration reaction can be determined over a range of temperature and used to determine the thermodynamics associated with ion hydration using the van't Hoff equation (110). However, it is challenging to coax water molecules to adsorb to singly-charged, gas-phase helices (110), presumably because the H-bonding network is too strong for water to penetrate. One potential way to overcome this obstacle is to begin the experiment with partially-desolvated ions. Finally, VT-IM-MS can be used to probe the interconversion of structural conformations and determine the kinetics of the rearrangement as a function of temperature (42). These experiments would be especially interesting for the AAKAA and AEAAKA peptides because bimodal distributions are observed at room temperature for $[M + H]^+$ and $[M + X]^+$ ions, respectively. By measuring the rate of interconversion as a function of temperature, the activation energy can be obtained from an Arrhenius plot.

IM-MS has shown great potential for biophysics and proteomics. IM-MS is a useful tool for studies of anhydrous biomolecules (*e.g.* proteins, peptides, DNA, etc.) (29; 59; 112). VT-IM-MS can be used to determine thermodynamic and kinetic information for structural interconversion and hydration. Application of IM-MS technology to novel and broadscale biophysical questions continues to drive future instrumental developments, pushing IM-MS into the forefront of modern biophysics and proteomics.

REFERENCES

1. Alberts, B., D. Bray, J. Lewis, M. Raff, K. Roberts, and J. D. Watson. 1994. Molecular biology of the cell. 3rd ed. Garland Publishing, Inc., New York.

2. Baldwin, R. L. 2005. Early days of studying the mechanism of protein folding. *In* Protein folding handbook, 1. Buchner J, Kiefhaber T, editors. Wiley-VCH Verlag, Weinheim. 3-21.

3. Levinthal, C. 1968. Are there pathways for protein folding? *J. Chim. Phys. Phys.-Chim. Biol.* 65:44-45.

4. Creighton, T. E. 1993. Proteins: Structures and molecular properties. 2nd ed. W. H. Freeman, New York.

5. Karplus, M., and D. L. Weaver. 1976. Protein-folding dynamics. *Nature* 260:404-406.

6. Kim, P. S., and R. L. Baldwin. 1982. Specific intermediates in the folding reactions of small proteins and the mechanism of protein folding. *Annu. Rev. Biochem.* 51:459-489.

7. Ptitsyn, O. B., and A. A. Rashin. 1975. A model of myoglobin self-organization. *Biophys. Chem.* 3:1-20.

8. Dill, K. A. 1985. Theory for the folding and stability of globular proteins. *Biochem.* 24:1501-1509.

9. Wetlaufer, D. B. 1973. Nucleation, rapid folding, and globular intrachain regions in proteins. *Proc. Natl. Acad. Sci.* 70:697-701.

10. Gianni, S., N. R. Guydosh, F. Khan, T. D. Caldas, U. Mayor, G. W. N. White, M. L. DeMarco, V. Daggett, and A. R. Fersht. 2003. Unifying features in protein-folding mechanisms. *Proc. Natl. Acad. Sci.* 100:13286-13291.

11. Hol, W. G. J., P. T. van Duijnen, and H. J. C. Berendsen. 1978. The α-helix dipole and the properties of proteins. *Nature* 273:443-446.

12. Chou, P. Y., and G. D. Fasman. 1978. Empirical predictions of protein conformation. *Annu. Rev. Biochem.* 47:251-276.

13. Wójcik, J., K. H. Altmann, and H. A. Scheraga. 1990. Helix-coil stability constants for the naturally occurring amino acids in water. XXIV. Half-cystine

parameters from random poly(hydroxybutylglutamine-co-S-methylthio-l-cysteine). *Biopolymers* 30:121-134.

14. Rohl, C. A., A. Chakrabartty, and R. L. Baldwin. 1996. Helix propagation and N-cap propensities of the amino acids measured in alanine-based peptides in 40 volume percent trifluoroethanol. *Protein Sci.* 5:2623-2637.

15. Lyu, P. C., M. I. Liff, L. A. Marky, and N. R. Kallenbach. 1990. Side chain contributions to the stability of alpha-helical structure in peptides. *Science* 250:669-673.

16. Pace, C. N., and J. M. Scholtz. 1998. A helix propensity scale based on experimental studies of peptides and proteins. *Biophys. J.* 75:422-427.

17. Avbelj, F., P. Luo, and R. L. Baldwin. 2000. Energetics of the interaction between water and the helical peptide group and its role in determining helix propensities. *Proc. Natl. Acad. Sci.* 97:10786-10791.

18. Luo, P., and R. L. Baldwin. 1999. Interaction between water and polar groups of the helix backbone: An important determinant of helix propensities. *Proc. Natl. Acad. Sci.* 96:4930-4935.

19. Pauling, L., R. B. Corey, and H. R. Branson. 1951. The structure of proteins: Two hydrogen-bonded helical configurations of the polypeptide chain. *Proc. Natl. Acad. Sci.* 37:205-211.

20. Jarrold, M. F. 2000. Peptides and proteins in the vapor phase. *Annu. Rev. Phys. Chem.* 51:179-207.

21. Wyttenbach, T., and M. T. Bowers. 2003. Gas-phase conformations: The ion mobility/ion chromatography method. *Top. Curr. Chem.* 225:207-232.

22. McLean, J. A., B. T. Ruotolo, K. J. Gillig, and D. H. Russell. 2005. Ion mobility–mass spectrometry: A new paradigm for proteomics. *Int. J. Mass Spectrom.* 240:301-315.

23. Valentine, S. J., A. E. Counterman, and D. E. Clemmer. 1999. A database of 660 peptide ion cross sections: Use of intrinsic size parameters for bona fide predictions of cross sections. *J. Am. Soc. Mass Spectrom.* 10:1188-1211.

24. Ruotolo, B. T., J. A. McLean, K. J. Gillig, and D. H. Russell. 2004. Peak capacity of ion mobility mass spectrometry: The utility of varying drift gas polarizability for the separation of tryptic peptides. *J. Mass Spectrom.* 39:361-367.

25. Tao, L., J. R. McLean, J. A. McLean, and D. H. Russell. 2007. A collision cross-section database of singly-charged peptide ions. *J. Am. Soc. Mass Spectrom.* In press.

26. von Helden, G., T. Wyttenbach, and M. T. Bowers. 1995. Conformation of macromolecules in the gas phase: Use of matrix-assisted laser desorption methods in ion chromatography. *Science* 267:1483-1485.

27. Wyttenbach, T., G. von Helden, and M. T. Bowers. 1996. Gas-phase conformation of biological molecules: Bradykinin. *J. Am. Chem. Soc.* 118:8355-8364.

28. Ruotolo, B. T., G. F. Verbeck, L. M. Thomson, K. J. Gillig, and D. H. Russell. 2002. Observation of conserved solution-phase secondary structure in gas-phase tryptic peptides. *J. Am. Chem. Soc.* 124:4214-4215.

29. Hudgins, R. R., M. A. Ratner, and M. F. Jarrold. 1998. Design of helices that are stable in vacuo. *J. Am. Chem. Soc.* 120:12974-12975.

30. Ruotolo, B. T., and D. H. Russell. 2004. Gas-phase conformations of proteolytically derived protein fragments: Influence of solvent on peptide conformation. *J. Phys. Chem. B* 108:15321-15331.

31. Ruotolo, B. T., G. F. Verbeck, L. M. Thomson, A. S. Woods, K. J. Gillig, and D. H. Russell. 2002. Distinguishing between phosphorylated and nonphophorylated peptides with ion mobility-mass spectrometry. *J. Proteome Res.* 1:303-306.

32. Ruotolo, B. T., K. J. Gillig, A. S. Woods, T. F. Egan, M. V. Ugarov, J. A. Schultz, and D. H. Russell. 2004. Analysis of phosphorylated peptides by ion mobility-mass spectrometry. *Anal. Chem.* 76:6727-6733.

33. McLean, J. A., J. R. McLean, and D. H. Russell, (2005) Anhydrous protein structures: The influence of post-translational modification on tertiary structures and evidence for protein aggregation. 19th Annual Symposium of the Protein Society.

34. McLean, J. R., J. A. McLean, L. M. Pérez, C. N. Pace, J. M. Scholtz, and D. H. Russell, (2005) Exploration of gas-phase peptide secondary structure using MALDI-IM-MS: Initial steps in the development of a gas-phase helical propensity scale. 53rd ASMS Conference on Mass Spectrometry.

35. Hudgins, R. R., Y. Mao, M. A. Ratner, and M. F. Jarrold. 1999. Conformations of Gly(n)H^+ and Ala(n)H^+ peptides in the gas phase. *Biophys. J.* 76:1591-1597.

36. Hudgins, R. R., and M. F. Jarrold. 1999. Helix formation in unsolvated alanine-based peptides: Helical monomers and helical dimers. *J. Am. Chem. Soc.* 121:3494-3501.

37. van Holde, E. K., W. C. Johnson, and P. S. Ho. 1998. Principles of physical biochemistry. Prentice Hall, Upper Saddle River.

38. Chakrabartty, A., A. J. Doig, and R. L. Baldwin. 1993. Helix capping propensities in peptides parallel those in proteins. *Proc. Natl. Acad. Sci.* 90:11332-11336.

39. Doig, A. J., and R. L. Baldwin. 1995. N- and C-capping preferences for all 20 amino acids in alpha-helical peptides. *Protein Sci.* 4:1325-1336.

40. Presta, L. G., and G. D. Rose. 1988. Helix signals in proteins. *Science* 240:1632-1641.

41. Kaleta, D. T., and M. F. Jarrold. 2001. Disrupting helix formation in unsolvated peptides. *J. Phys. Chem. B* 105:4436-4440.

42. Kinnear, B. S., M. R. Hartings, and M. F. Jarrold. 2001. Helix unfolding in unsolvated peptides. *J. Am. Chem. Soc.* 123:5660-5667.

43. Hudgins, R. R., M. Imai, and M. F. Jarrold. 1999. High-resolution ion mobility measurements for silicon cluster anions and cations. *J. Chem. Phys.* 111:7865-7870.

44. Hudgins, R. R., and M. F. Jarrold. 2000. Conformations of unsolvated glycine-based peptides. *J. Phys. Chem. B* 104:2154-2158.

45. Chakrabartty, A., and R. L. Baldwin. 1995. Stability of alpha-helices. *Adv. Protein Chem.* 46:141-176.

46. Piela, L., G. Nemethy, and H. A. Scheraga. 1987. Conformational constraints of amino acid side chains in alpha-helices. *Biopolymers* 26:1273-1286.

47. Creamer, T. P., and G. D. Rose. 1992. Side-chain entropy opposes alpha-helix formation but rationalizes experimentally determined helix-forming propensities. *Proc. Natl. Acad. Sci.* 89:5937-5941.

48. Kinnear, B. S., and M. F. Jarrold. 2001. Helix formation in unsolvated peptides: Side chain entropy is not the determining factor. *J. Am. Chem. Soc.* 123:7907-7908.

49. Kohtani, M., B. S. Kinnear, and M. F. Jarrold. 2000. Metal-ion enhanced helicity in the gas phase. *J. Am. Chem. Soc.* 122:12377-12378.

50. Kohtani, M., M. F. Jarrold, S. Wee, and R. A. J. O'Hair. 2004. Metal ion interactions with polyalanine peptides. *J. Phys. Chem. B* 108:6093-6097.

51. Figueroa, I. D., and D. H. Russell. 1999. Matrix-assisted laser desorption ionization hydrogen/deuterium exchange studies to probe peptide conformational changes. *J. Am. Soc. Mass Spectrom.* 10(8):719-731.

52. Ruotolo, B. T., C. C. Tate, and D. H. Russell. 2004. Ion mobility-mass spectrometry applied to cyclic peptide analysis: Conformational preferences of gramicidin S and linear analogs in the gas phase. *J. Am. Soc. Mass Spectrom.* 15:870-878.

53. Sawyer, H. A., J. T. Marini, E. G. Stone, B. T. Ruotolo, K. J. Gillig, and D. H. Russell. 2005. The structure of gas-phase bradykinin fragment 1-5 (RPPGF) ions: An ion mobility spectrometry and H/D exchange ion-molecule reaction chemistry study. *J. Am. Soc. Mass Spectrom.* 16:893-905.

54. Scholtz, J. M., H. Qian, E. J. York, J. M. Stewart, and R. L. Baldwin. 1991. Parameters of helix-coil transition theory for alanine-based peptides of varying chain lengths in water. *Biopolymers* 31:1463-1470.

55. Rohl, C. A., J. M. Scholtz, E. J. York, J. M. Stewart, and R. L. Baldwin. 1992. Kinetics of amide proton exchange in helical peptides of varying chain lengths. Interpretation by the Lifson-Roig equation. *Biochem.* 31:1263-1269.

56. Marqusee, S. M., and R. L. Baldwin. 1987. Helix stabilization by $Glu^{-}.Lys^{+}$ salt bridges in short peptides of *de novo* design. *Proc. Natl. Acad. Sci.* 84:8898-8902.

57. Marqusee, S. M., V. H. Robbins, and R. L. Baldwin. 1989. Unusually stable helix formation in short alanine-based peptides. *Proc. Natl. Acad. Sci.* 86:5286-5290.

58. Takahashi, S., E. H. Kim, T. Hibino, and T. Ooi. 1989. Comparison of alpha-helix stability in peptides having a negatively or positively charged residue block attached either to the N- or C-terminus of an alpha-helix: The electrostatic contribution and anisotropic stability of the alpha-helix. *Biopolymers* 28:995-1009.

59. Clemmer, D. E., R. R. Hudgins, and M. F. Jarrold. 1995. Naked protein conformations: Cytochrome C in the gas phase. *J. Am. Chem. Soc.* 117:10141-10142.

60. Shelimov, K. B., and M. F. Jarrold. 1997. Conformations, unfolding, and refolding of apomyoglobin in vacuum: An activation barrier for gas-phase protein folding. *J. Am. Chem. Soc.* 119:2987-2994.

61. Gillig, K. J., B. T. Ruotolo, E. G. Stone, D. H. Russell, K. Fuhrer, M. Gonin, and J. A. Schultz. 2000. Coupling high-pressure MALDI with ion mobility/orthogonal time-of-flight mass spectrometry. *Anal. Chem.* 72:3965-3971.

62. McLean, J. A., and D. H. Russell. 2003. Sub-femtomole peptide detection in ion mobility-time-of-flight mass spectrometry measurements. *J. Proteome Res.* 2:427-430.

63. Mason, E. A., and E. W. McDaniel. 1988. Transport properties of ions in gases. Wiley, New York, NY.

64. Revercomb, H. E., and E. A. Mason. 1975. Theory of plasma chromatography/gaseous electrophoresis--a review. *Anal. Chem.* 47:970-983.

65. Mesleh, M. F., J. M. Hunter, A. A. Shvartsburg, G. C. Schatz, and M. F. Jarrold. 1996. Structural information from ion mobility measurements: Effects of the long-range potential. *J. Phys. Chem.* 100:16082-16086.

66. Ruotolo, B. T., J. A. McLean, K. J. Gillig, and D. H. Russell. 2005. The influence and utility of varying field strength for the separation of tryptic peptides by ion mobility-mass spectrometry. *J. Am. Soc. Mass Spectrom.* 16:158-165.

67. Crank, J. 1975. The mathematics of diffusion. 2nd ed. Oxford University Press, Oxford.

68. Raznikov, V. V., I. V. Soulimenkov, V. I. Kozlovski, A. R. Pikhtelev, M. O. Raznikova, T. Horwath, A. A. Kholomeev, Z. Zhou, H. Wollnik, and A. F. Dodonov. 2001. Ion rotating motion in a gas-filled radio-frequency quadrupole ion guide as a new technique for structural and kinetic investigations of ions. *Rapid Commun. Mass Spectrom.* 15:1912-1921.

69. Jarrold, M. F., and E. C. Honea. 1991. Dissociation of large silicon clusters: The approach to bulk behavior. *J. Phys. Chem.* 95:9181-9185.

70. Insight II (Accelrys, San Diego, CA).

71. Cerius^2 (Accelrys, San Diego, CA).

72. Hunter, E. P., and S. G. Lias. 1998. Evaluated gas phase basicities and proton affinities of molecules: An update. *J. Phys. Chem. Ref. Data* 27:413-656.

73. Berendsen, H. J. C., J. P. M. Postma, W. F. van Gunsteren, A. DiNola, and J. R. Haak. 1984. Molecular dynamics with coupling to an external bath. *J. Chem. Phys.* 81:3684-3690.

74. Delano, W. L. (2006) The pymol molecular graphics system (DeLano Scientific). http://www.pymol.org.

75. Kabsch, W., and C. Sander. 1983. Dictionary of protein secondary structure: Pattern recognition of hydrogen-bonded and geometrical features. *Biopolymers* 22:2577-2637.

76. Eiceman, G. A., and Z. Karpas. 2005. Ion mobility spectrometry. 2nd ed. CRC Press, Boca Raton.

77. Hoaglund-Hyzer, C. S., A. E. Counterman, and D. E. Clemmer. 1999. Anhydrous protein ions. *Chem. Rev.* 99:3037-3080.

78. Breaux, G. A., and M. F. Jarrold. 2003. Probing helix formation in unsolvated peptides. *J. Am. Chem. Soc.* 125:10740-10747.

79. Kohtani, M., J. E. Schneider, T. C. Jones, and M. F. Jarrold. 2004. The mobile proton in polyalanine peptides. *J. Am. Chem. Soc.* 126:16981-16987.

80. Hilderbrand, A. E., and D. E. Clemmer. 2005. Determination of sequence-specific intrinsic size parameters from cross sections for 162 tripeptides. *J. Phys. Chem. B* 109:11802-11809.

81. White, S. H., and W. C. Wimley. 1999. Membrane protein folding and stability: Physical principles. *Annu. Rev. Biophys. Biomol. Struct.* 28:319-365.

82. Kibanov, A. M. 2001. Improving enzymes by using them in organic solvents. *Nature* 409:241-246.

83. Mattos, C., and D. Ringe. 2001. Proteins in organic solvents. *Curr. Opin. Struct. Biol.* 11:761-764.

84. Sudha, R., M. Kohtani, G. A. Breaux, and M. F. Jarrold. 2004. Pi-helix preference in unsolvated peptides. *J. Am. Chem. Soc.* 126:2777-2784.

85. Counterman, A. E., and D. E. Clemmer. 2001. Large anhydrous polyalanine ions: Evidence for extended helices and onset of a more compact state. *J. Am. Chem. Soc.* 123:1490-1498.

86. Kohtani, M., T. C. Jones, J. E. Schneider, and M. F. Jarrold. 2004. Extreme stability of an unsolvated alpha-helix. *J. Am. Chem. Soc.* 126:7420-7421.

87. Di Cera, E. 2006. A structural perspective on enzymes activated by monovalent cations. *J. Biol. Chem.* 281:1305-1308.

88. Page, M. J., and E. Di Cera. 2006. Role of Na^+ and K^+ in enzyme function. *Physiological Reviews* 86:1049-1092.

89. Yernool, D., O. Boudker, Y. Jin, and E. Gouaux. 2004. Structure of a glutamate transporter homologue from pyrococcus horikoshii. *Nature* 431:811.

90. Boudker, O., R. M. Ryan, D. Yernool, K. Shimamoto, and E. Gouaux. 2007. Coupling substrate and ion binding to extracellular gate of a sodium-dependent aspartate transporter. *Nature* 445:387-393.

91. Zhou, Y., J. H. Morais-Cabral, A. Kaufman, and R. MacKinnon. 2001. Chemistry of ion coordination and hydration revealed by a K^+ channel-Fab complex at 2.0 angstrom resolution. *Nature* 414:43-48.

92. Doyle, D. A., J. Morais Cabral, R. A. Pfuetzner, A. Kuo, J. M. Gulbis, S. L. Cohen, B. T. Chait, and R. MacKinnon. 1998. The structure of the potassium channel: Molecular basis of K^+ conduction and selectivity. *Science* 280:69-77.

93. Roux, B., and R. MacKinnon. 1999. The cavity and pore helices in the KcsA K^+ channel: Electrostatic stabilization of monovalent cations. *Science* 285:100-102.

94. McLean, J. R., J. A. McLean, L. M. Perez, C. N. Pace, J. M. Scholtz, and D. H. Russell. 2007. Helical preferences for model peptide ions containing multiple basic sites: A combined experimental and molecular modeling study. *J. Am. Chem. Soc.* submitted.

95. Olsher, U. 1991. Coordination chemistry of lithium ion: A crystal and molecular structure review. *Chem. Rev.* 91:137-164.

96. Ramachandran, G. N., and V. Sasisekharan. 1968. Conformation of polypeptides and proteins. *Adv. Protein Chem.* 23:283-438.

97. Goldenberg, D. P. 2003. Computational simulation of the statistical properties of unfolded proteins. *J. Mol. Biol.* 326:1615-1633.

98. Petrescu, A. J., P. Calmettes, D. Durand, V. Receveur, and J. C. Smith. 2000. Change in backbone torsion angle distribution on protein folding. *Protein Sci.* 9:1129-1136.

99. Gilson, M. K., and B. H. Honig. 1986. The dielectric constant of a folded protein. *Biopolymers* 25:2097-2119.

100. Antosiewicz, J., J. A. McCammon, and M. K. Gilson. 1994. Prediction of pH-dependent properties of proteins. *J. Mol. Biol.* 238:415-436.

101. Valentine, S. J., and D. E. Clemmer. 2002. Temperature-dependent H/D exchange of compact and elongated cytochrome c ions in the gas phase. *J. Am. Soc. Mass Spectrom.* 13:506-517.

102. Figueroa, I. D., O. Torres, and D. H. Russell. 1998. Effects of the water content in the sample preparation for MALDI on the mass spectra. *Anal. Chem.* 70(21):4527-4533.

103. Hattan, S. J., J. Marchese, M. Albertinetti, S. Krishnan, N. Khainovski, and P. Juhasz. 2004. Effect of solvent composition on signal intensity in liquid chromatography-matrix-assisted laser desorption ionization experiments. *J Chromatogr A* 1053:291-297.

104. Luo, G., I. Marginean, and A. Vertes. 2002. Internal energy of ions generated by matrix-assisted laser desorption/ionization. *Anal. Chem.* 74:6185-6190.

105. Elizabeth Stevenson, K. B. R. Z. 2000. Internal energies of analyte ions generated from different matrix-assisted laser desorption/ionization matrices. *J. Mass Spectrom.* 35:1035-1041.

106. Kohtani, M., T. C. Jones, R. Sudha, and M. F. Jarrold. 2006. Proton transfer-induced conformational changes and melting in designed peptides in the gas phase. *J. Am. Chem. Soc.* 128:7193-7197.

107. Baumketner, A., S. L. Bernstein, T. Wyttenbach, N. D. Lazo, D. B. Teplow, M. T. Bowers, and J. E. Shea. 2006. Structure of the 21-30 fragment of amyloid beta-protein. *Protein Sci.* 15:1239-1247.

108. Koeniger, S. L., S. I. Merenbloom, and D. E. Clemmer. 2006. Evidence for many resolvable structures within conformation types of electrosprayed ubiquitin ions. *J. Phys. Chem. B* 110:7017-7021.

109. Mao, Y., M. A. Ratner, and M. F. Jarrold. 2000. One water molecule stiffens a protein. *J. Am. Chem. Soc.* 122:2950-2951.

110. Kohtani, M., and M. F. Jarrold. 2002. The initial steps in the hydration of unsolvated peptides: Water molecule adsorption on alanine-based helices and globules. *J. Am. Chem. Soc.* 124:11148-11158.

111. Kohtani, M., and M. F. Jarrold. 2004. Water molecule adsorption on short alanine peptides: How short is the shortest gas-phase alanine-based helix? *J. Am. Chem. Soc.* 126:8454-8458.

112. Gidden, J., A. Ferzoco, E. S. Baker, and M. T. Bowers. 2004. Duplex formation and the onset of helicity in poly d(CG)n oligonucleotides in a solvent-free environment. *J. Am. Chem. Soc.* 126:15132-15140.

VITA

Janel Renée McLean

EDUCATION

Texas A & M University, College Station, Texas	2007
Ph.D. Bioanalytical Chemistry	
Cornell University, Ithaca, New York	2003
M.S. Environmental Toxicology and Molecular Medicine	
Advisors: Randolph C. Elble and Bendicht U. Pauli.	
Maryville College, Maryville, Tennessee	2000
B.A. Biology and Chemistry, *Magna Cum Laude*	
Advisors: Terry Bunde and Paul Threadgill	
West Carrollton High School, West Carrollton, Ohio	1996
Valedictorian	

HONORS AND AWARDS

Martin Corera Travel Award recipient (TAMU)	2006
Phi Lambda Upsilon Chemistry Honor Society (TAMU)	2005-
Magna Cum Laude (MC)	2000
Senior Award in Chem. (MC)	2000
Alpha Gamma Sigma, Senior Honor Society (MC)	1996-
Elizabeth J. Hillman Chem. Award (MC)	1999
Outstanding Performance in Structural Chem. Award (MC)	1998
Outstanding Performance in Introductory Chem. Award (MC)	1997
Presidential Scholar (MC)	1996-2000
Dean’s List (MC)	1996-2000
Alpha Lambda Delta, Freshman Honor Society (MC)	1996-

LEADERSHIP AND OUTREACH

Judge for Student Research Week (TAMU)	2005
Assoc. for Comparative Environ. Tox. Students, Treasurer (CU)	2001-2003
Student Government Association Junior Class Senator (MC)	1998-1999
Environmental Action Team, Founder and Board Rep. (MC)	1998-1999
Student Government Environmental Committee Member (MC)	1997-1998
Alpha Lamda Delta, Vice President (MC)	1997-1998

PROFESSIONAL AFFILIATIONS

American Chemical Society
American Society for Mass Spectrometry
Biophysical Society
Protein Society
Society for Analytical Spectroscopy